

$p$  is the pion momentum, and  $\alpha$  is the fundamental length. Our value of the lifetime for pions in flight and the William and Mary measurement with stopping pions place an upper limit on  $\alpha$  of  $3 \times 10^{-15}$  cm.

### ACKNOWLEDGMENTS

We would like to express our appreciation to Professor A. Carl Helmholz and Professor Burton J. Moyer for their support and encouragement throughout this work. We thank James Vale and the entire cyclotron staff for trouble-free machine operation. Particular thanks go to Lloyd B. Houser, Donald F. Rothfuss, and Louis A.

Sylvia for their help with the design, installation, and smooth operation of the experimental equipment. We appreciate the assistance of Cordon R. Kerns with photomultiplier problems. The liquid-deuterium Čerenkov counters owe their success to Albert H. Kleid who assembled the flasks, Edwin F. McLaughlin, and Richard V. Schafer who were responsible for the cryogenic design and operation of the counters, and Rene Bollaert, Russell F. Ellis, and Allan R. Susoeff of the hydrogen-target group, whose hard work kept both counters working properly. We are grateful to Dr. Richard J. Kurz for his help in the early stages of the design.

## Reaction $pp \rightarrow pp\pi^+\pi^-$ at 6.6 GeV/c\*

EUGENE COLTON† AND PETER E. SCHLEIN‡

*Department of Physics, University of California, Los Angeles, California 90024*

AND

EUGENE GELLERT

*Lawrence Radiation Laboratory, Berkeley, California 94720*

AND

GERALD A. SMITH

*Department of Physics, Michigan State University, East Lansing, Michigan 48823*

(Received 31 August 1970)

A detailed analysis of 7514  $pp \rightarrow pp\pi^+\pi^-$  events at 6.6-GeV/c incident beam momentum is presented. Three types of analyses are presented which argue that a single-pion exchange process is responsible for the dominant peripheral  $\Delta^+\pi^-$  production. An angular-correlation analysis is presented in which it appears that the 1450-MeV  $\Delta\pi$  Deck enhancement is not a pure  $J^P = \frac{1}{2}^+$  state. The demonstration that the absolute magnitude for this enhancement is accounted for by the pion-exchange process indicates that only one process (i.e., pion exchange with diffraction scattering at the  $\pi^-p$  vertex) contributes to the final state, and that a second process need not be added to the pion exchange to account for the observed cross section. Some *ad hoc* dependence on the  $\Delta\pi$  mass must be introduced for a precise fit to the *shape* of the  $\Delta\pi$  mass spectrum, or equivalently to the  $\theta, \phi$  angular distributions in the  $\pi^-p$  c.m. system. The  $s_{\Delta\pi}^{2\alpha(t)}$  dependence of the Reggeized pion-exchange model of Berger is well known to accomplish this; however, the  $\alpha(t)$  with unit slope required by this model is at variance with the apparently rather flat trajectory deduced from data on quasi-two-body pion-exchange-dominated reactions. It is suggested that a  $\Delta\pi$  final-state-interaction model may be useful in understanding the reaction.

### I. INTRODUCTION

A GENERAL feature of proton-proton inelastic scattering in the intermediate- and high-energy regions is the preference for production with small momentum transfer. In order to study some of the characteristics of these peripheral processes, we have analyzed 7514 events of the type

$$pp \rightarrow pp\pi^+\pi^- \quad (1)$$

at an incident laboratory momentum of 6.6 GeV/c

(3.77-GeV total c.m. energy). Data for reaction (1) have been previously presented at incident beam momenta of 2.23,<sup>1</sup> 2.81,<sup>2</sup> 3.68,<sup>3</sup> 4.0,<sup>4</sup> 5.0,<sup>5</sup> 5.5,<sup>6</sup>

<sup>1</sup> A. M. Eisner, E. L. Hart, R. I. Loutitt, and T. W. Morris, Phys. Rev. **138**, B670 (1965).

<sup>2</sup> W. J. Fickinger, E. Pickup, D. K. Robinson, and E. O. Salant, Phys. Rev. **125**, 2082 (1962).

<sup>3</sup> E. L. Hart, R. I. Loutitt, D. Luers, T. W. Morris, W. J. Willis, and S. S. Yamamoto, Phys. Rev. **126**, 747 (1962).

<sup>4</sup> L. Bodini, L. Casé, J. Kidd, L. Mandelli, V. Pelosi, S. Ratti, V. Russo, L. Tallone, C. Caso, F. Conte, M. Dameri, and G. Tomasini, Nuovo Cimento **58A**, 475 (1968).

<sup>5</sup> E. P. Colleraine and U. Nauenberg, Phys. Rev. **161**, 1387 (1967).

<sup>6</sup> G. Alexander, O. Benary, G. Czapek, B. Haber, N. Kidron, B. Reuter, A. Shapira, E. Simopoulou, and G. Yekutieli, Phys. Rev. **154**, 1284 (1967); see also G. Yekutieli *et al.*, Nucl. Phys. **B18**, 301 (1970).

\* Supported in part by the U. S. Atomic Energy Commission.

† Present address: Lawrence Radiation Laboratory, Berkeley, Calif. 94720.

‡ John Simon Guggenheim Memorial Fellow, presently on sabbatical leave at CERN, Geneva.

6.0,<sup>7,8</sup> 6.6,<sup>9-12</sup> 6.9,<sup>6</sup> 7.9,<sup>13</sup> 8.1,<sup>14</sup> 10.0,<sup>15</sup> 16.0,<sup>16</sup> 19.0,<sup>17</sup> 21.8,<sup>18</sup> 24.8,<sup>19</sup> and 28.5<sup>20,21</sup> GeV/c.

Our previous publications,<sup>9-12</sup> which have been based on part or all of our final sample for reaction (1), have dealt with the following subjects:

- (a)<sup>9</sup> Isobar production in  $pp \rightarrow pp\pi^+\pi^-$ .
- (b)<sup>10</sup> Reggeized Deck-model fits to  $pp \rightarrow \Delta^{++}p\pi^-$ .
- (c)<sup>11</sup> One-pion-exchange analysis of  $pp \rightarrow \Delta^{++}p\pi^-$ .
- (d)<sup>12</sup> Comparison between off- and on-shell inelastic  $\pi^-p$  scattering.

In the present article we summarize the previous work, expand and elaborate on many of the points made, and attempt to arrive at some form of coherent picture of the production mechanism of the dominant  $\Delta^{++}p\pi^-$  channel in reaction (1).

Reaction (1) is dominated by peripheral  $\Delta^{++}(1238)$  production. In the analysis which follows we attempt to arrive at some understanding of the production mechanism of the peripheral  $\Delta^{++}(1238)$ ,  $p\pi^+\pi^-$ , and  $\Delta^{++}(1238)\pi^-$  systems at 6.6 GeV/c.

In Sec. II we discuss the beam, scanning, measuring, and separation procedures which were used to obtain our data sample of  $pp\pi^+\pi^-$  events. The production cross section for reaction (1) at 6.6 GeV/c is presented

<sup>7</sup> C. Caso, F. Conte, G. Tomasini, L. Casé, L. Mosca, S. Ratti, L. Tallone-Lombardi, I. Bloodworth, L. Lyons, and A. Norton, *Nuovo Cimento* **55A**, 66 (1968).

<sup>8</sup> W. Chinowsky, P. Condon, R. R. Kinsey, S. Klein, M. Mandelkern, P. Schmidt, J. Schultz, F. Martin, M. L. Perl, and T. H. Tan, *Phys. Rev.* **171**, 1421 (1968).

<sup>9</sup> E. Gellert, G. A. Smith, S. J. Wojcicki, E. Colton, P. E. Schlein, and H. K. Ticho, *Phys. Rev. Letters* **17**, 884 (1966).

<sup>10</sup> E. L. Berger, E. Gellert, G. A. Smith, E. Colton, and P. E. Schlein, *Phys. Rev. Letters* **20**, 964 (1968).

<sup>11</sup> E. Colton, P. E. Schlein, E. Gellert, and G. A. Smith, University of California, Los Angeles, Report No. UCLA-1023-Rev.

<sup>12</sup> E. Colton, P. E. Schlein, E. Gellert, and G. A. Smith, *Phys. Rev. Letters* **21**, 1548 (1968).

<sup>13</sup> D. Grether, G. Ascoli, M. Firebaugh, E. L. Goldwasser, R. D. Sard, and J. Wray, *Bull. Am. Phys. Soc.* **12**, 10 (1967).

<sup>14</sup> G. Kayas, J. Le Guyader, M. Senl, T. P. Yiow, J. Alitti, Ngeiyen Thuc Diem, G. Smadja, J. Ginestet, D. Manesse, and Tram Ha Anh, *Nucl. Phys.* **B5**, 169 (1968).

<sup>15</sup> S. P. Almeida, J. G. Rushbrooke, J. H. Scharenguivel, M. Behrens, V. Blobel, I. Borecka, H. C. Dehne, J. Diaz, G. Knies, A. Schmitt, K. Strömer, and W. P. Swanson, *Phys. Rev.* **174**, 1638 (1968).

<sup>16</sup> J. G. Rushbrooke, and J. R. Williams, *Phys. Rev. Letters* **22**, 248 (1969).

<sup>17</sup> H. Bøggild, J. Eades, K. Hansen, H. Johnstad, R. Möllerard, L. Veje, P. Laurikainen, P. Lindblom, J. Tuominiemi, T. Jacobsen, S. O. Sørensen, Ö. Thingrold, G. Ekspong, L. Granström, S. O. Holmgren, S. Nilsson, T. Olhede, V. Svedin, and N. Yamdagni, in *Proceedings of the Fourteenth International Conference on High-Energy Physics, Vienna, 1968*, edited by J. Prentki and J. Steinberger (CERN, Geneva, 1968).

<sup>18</sup> R. A. Jespersen, Y. W. Kang, W. J. Kernan, R. A. Leacock, J. I. Rhode, T. L. Schalk, and L. S. Schroeder, *Phys. Rev. Letters* **21**, 1368 (1968).

<sup>19</sup> R. Ehrlich, R. Nieporent, R. J. Plano, J. B. Whittaker, C. Baltay, J. Feinman, P. Franzini, R. Newman, and N. Yeh, *Phys. Rev. Letters* **21**, 1839 (1968).

<sup>20</sup> W. E. Ellis, D. J. Miller, T. W. Morris, R. S. Panvini, and A. M. Thorndike, *Phys. Rev. Letters* **21**, 697 (1968).

<sup>21</sup> P. L. Connolly, W. E. Ellis, P. V. C. Hough, D. J. Miller, T. W. Morris, C. Ouannes, R. S. Panvini, and A. M. Thorndike, in *Third Topical Conference on Resonant Particles*, Athens, Ohio, 1967 (unpublished).

in Sec. III. The c.m. angular and four-momentum transfer distributions of each final-state particle are presented in Sec. IV. In Sec. V we present the two- and three-body invariant-mass distributions for the entire sample of 7514  $pp \rightarrow pp\pi^+\pi^-$  events. In Sec. VI we discuss the properties of the peripheral  $p\pi^+\pi^-$  system from the standpoint of direct resonance production. In Sec. VII we discuss the non- $\Delta^{++}$  events. The  $\Delta^{++}(1238)$  production is analyzed in some detail in Sec. VIII. Discussions of fits of single-particle exchange and multiperipheral exchange models to the data are presented. These results form the main body of the paper. Our conclusions are stated in Sec. IX.

## II. EXPERIMENTAL PROCEDURES

The data were obtained in an exposure of the Lawrence Radiation Laboratory 72-in. hydrogen bubble chamber to the P65 separated proton beam<sup>22</sup>; 493 000 pictures were obtained at incident momenta of 5.45 and 6.6 GeV/c. The momentum spread of the beam was about  $\pm 0.15\%$ <sup>22</sup>; the pion contamination was less than 0.1%.<sup>22</sup>

The film was scanned twice for events with four-prong topology. Events with kinking tracks were ignored unless the decay was  $\pi\mu e$ . The two-scan detection efficiency was 99.4%.

Each measured event was required to fit the hypothesis of reaction (1) with  $\chi^2$  probability  $> 10^{-6}$ .

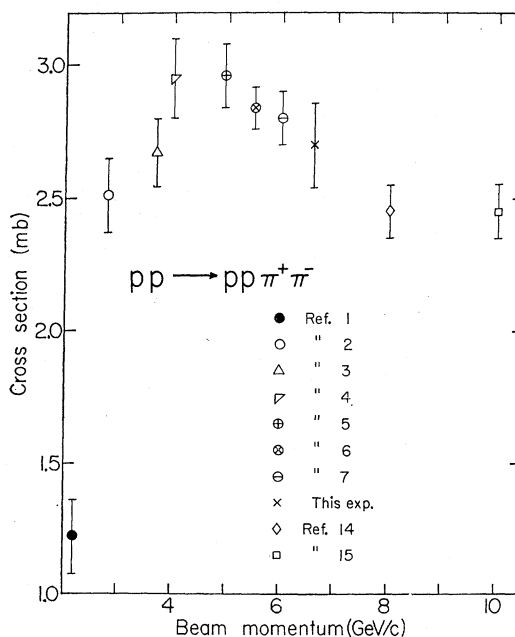


FIG. 1. Production cross section for  $pp \rightarrow pp\pi^+\pi^-$  as a function of the laboratory momentum of the incident beam.

<sup>22</sup> W. Chinowsky, R. R. Kinsey, S. L. Klein, M. Mandelkern, J. Schultz, F. Martin, M. L. Perl, and T. H. Tan, *Phys. Rev.* **165**, 1466 (1968).

Ambiguities with other hypotheses and track ambiguities were resolved by visually inspecting the bubble density of the tracks if the event was measured on an SMP or Franckenstein measuring machine. The pulse-height information for the darkness of tracks was used if the event was measured on the Spiral Reader. If the  $\chi^2$  and ionization criteria were insufficient to separate different hypotheses within a certain constraint class, the fit with lowest  $\chi^2$  was assumed to be the correct one. 7514 examples of reaction (1) resulted from the measurements which satisfied beam-track requirements. The contamination from all other reactions [or reaction (1) with incorrect track identification] in this sample was estimated to be  $(2 \pm 1)\%$  in a study of a subsample of the events.

### III. TOTAL CROSS SECTION

The total cross section obtained for reaction (1) at 6.6 GeV/c is  $2.70 \pm 0.16$  mb. The cross section was determined in a study of a subsample of 10 rolls of film. The error is due to the error in the path length ( $\pm 3.9\%$ ) and the statistical uncertainty in the number of events ( $\pm 4.5\%$ ). The cross section for reaction (1) as obtained in this experiment is consistent with values obtained at nearby incident beam momenta in other experiments. Figure 1 shows the cross section for reaction (1) plotted as a function of the laboratory momentum of the incident beam.<sup>1-15</sup>

### IV. SINGLE-PARTICLE DISTRIBUTIONS

The distributions of the c.m. longitudinal momenta for proton,  $\pi^+$ , and  $\pi^-$  are given in Figs. 2(a)–2(c),

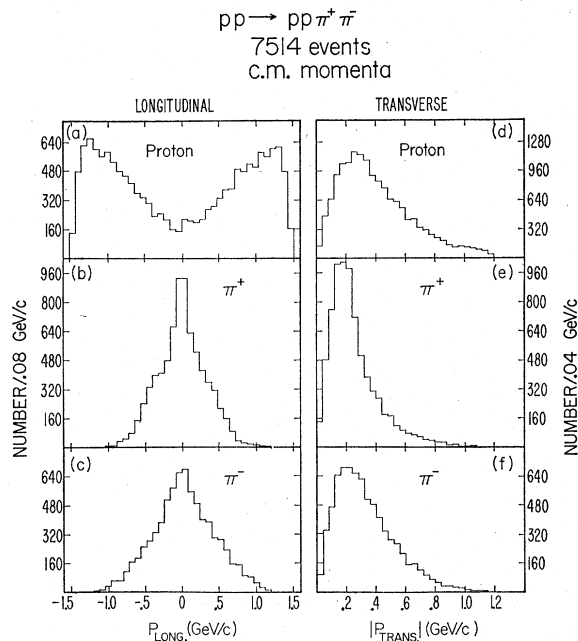


FIG. 2. (a)–(c): Distributions of c.m. longitudinal momenta of proton,  $\pi^+$ , and  $\pi^-$ , respectively, for the 7514  $pp\pi^+\pi^-$  events. (d)–(f): The corresponding spectra of c.m. transverse momenta.

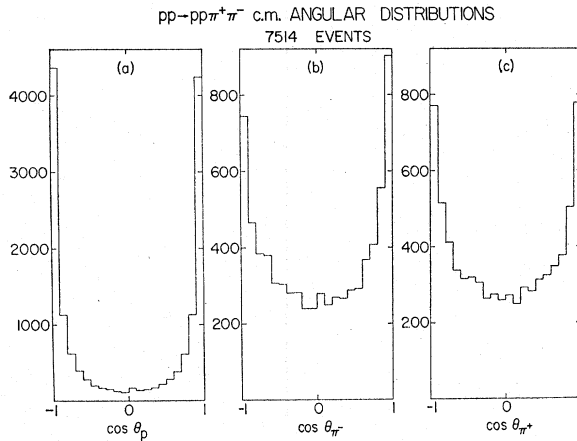


FIG. 3. c.m. angular distributions for the 7514  $pp\pi^+\pi^-$  events; (a) proton, (b)  $\pi^-$ , and (c)  $\pi^+$ .

respectively. Each event is plotted twice in Fig. 2(a). The gross features indicate that the protons tend to be produced with large values of longitudinal momenta while the pions prefer to center at zero longitudinal momenta. The  $\pi^+$  distribution [Fig. 2(b)] has a smaller width than the  $\pi^-$  distribution [Fig. 2(c)].

The corresponding spectra of transverse momenta are given in Figs. 2(d)–2(f). The pion distributions peak around 200 MeV/c, while the broader proton distribution peaks in the neighborhood of 300 MeV/c. As is the case with the longitudinal momentum, the transverse distribution for the  $\pi^+$  is also narrower than that of the  $\pi^-$ .

The distributions in Fig. 2 indicate that the protons prefer to be emitted in fast forward/backward cones of small apex angle about the beam direction. The pions, on the other hand, prefer to be emitted equatorially in the c.m. system with low momenta.

The c.m. angular distributions for proton,  $\pi^-$ , and  $\pi^+$  are displayed in Figs. 3(a)–3(c), respectively. As noted above, the proton distribution peaks steeply in the forward and backward directions. The  $\pi^+$  and proton distributions are fore-aft symmetric, as they should be because of the symmetric initial state. We believe that the small asymmetry observed for the  $\pi^-$  is a combination of a statistical fluctuation and a small bias against slow  $\pi^-$  in the lab. The effect is a small percentage effect and does not affect any of the physics results in this paper.

The corresponding momentum transfer distributions for proton,  $\pi^-$ , and  $\pi^+$  are given in Figs. 4(a)–4(c). We define  $t$  as the negative of the four-momentum transfer squared from the incoming beam particle to the outgoing particle. The proton  $t$  distribution is folded in Fig. 4(a). For each outgoing proton there are two values of  $t$  which can be calculated with respect to an incident proton. We take the lower of the two values to be the correct one. This procedure associates an outgoing proton with the incident proton which propa-

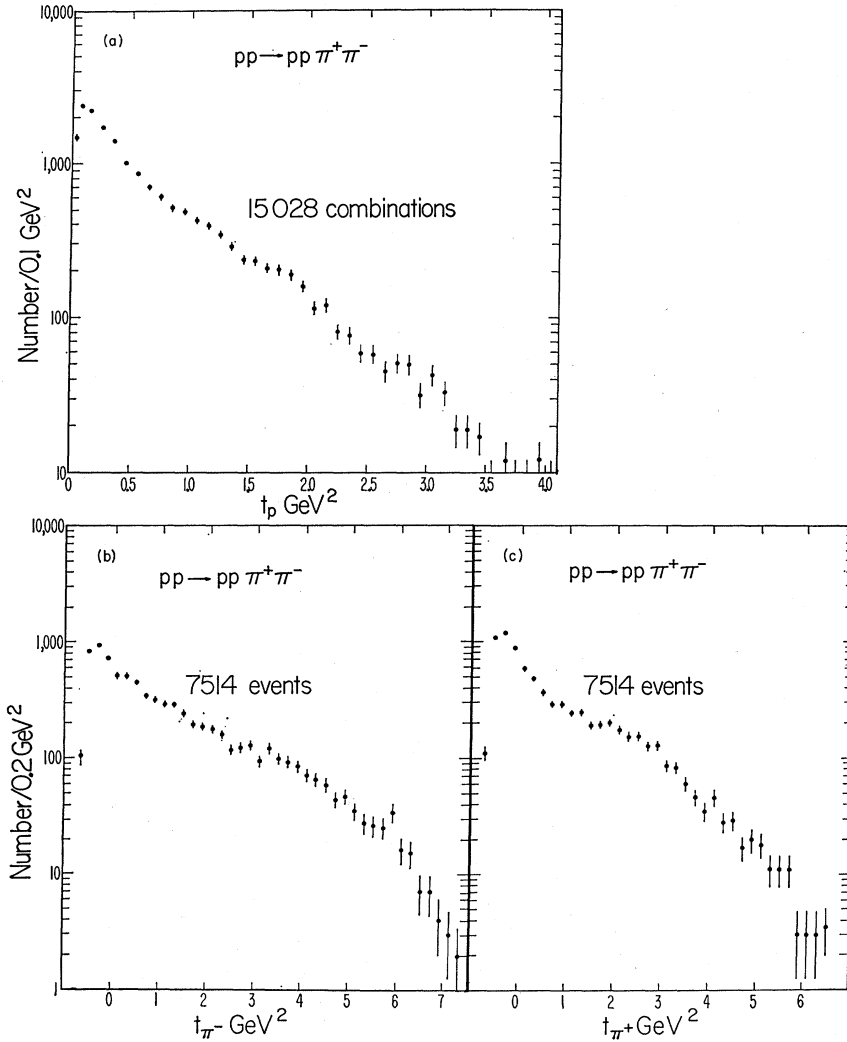


FIG. 4. Distributions of four-momentum transfer squared for the 7514  $pp\pi^+\pi^-$  events; (a) proton, (b)  $\pi^-$ , and (c)  $\pi^+$ .

gates in the same hemisphere in the c.m. system. The preference for low-momentum transfer indicates that peripheral-production mechanisms play a major role in these events.

### V. INVARIANT-MASS SPECTRA

The distributions of invariant mass for the 7514  $pp\pi^+\pi^-$  events are given in Figs. 5–8. They are  $M(p\pi^+)$  (Fig. 5 with two combinations per event),  $M(p\pi^-)$  and  $M(p\pi^+\pi^-)$  [Figs. 6(a) and 6(b), each with two combinations per event],  $M(\pi^+\pi^-)$  and  $M(pp)$  [Figs. 7(a) and 7(b)], and the  $M(pp\pi^-)$  and  $M(pp\pi^+)$  [Figs. 8(a) and 8(b)]. The smooth curves drawn on Figs. 7 and 8 are the predictions of four-body phase space. The phase-space calculations are unrealistic since they assume isotropy in the c.m. angular distributions and no resonance production.

In Fig. 5 the curve labeled *A* is the phase-space prediction while the *B* curve is the prediction of phase

space modified by the Breit-Wigner function

$$f_{BW} \equiv \frac{1}{|(M_{\Delta} - M)/\frac{1}{2}\Gamma|^2 + 1} \quad (2)$$

40% of the time [i.e., the factor  $(0.6 + 0.4 f_{BW})$  multiplies the phase-space distribution];  $M$  is the mass of the  $p\pi^+$  system. In the calculation  $M_{\Delta}$  was set equal to 1.21 GeV and  $\Gamma$ , the full width at half-maximum (FWHM), was fixed at 0.110 GeV. The *B* curve fits the  $p\pi^+$  mass distribution very well. If reaction (1) involved  $\Delta^{++}(1238)$  production 100% of the time, we should expect 50% of the area enclosed by the histogram in Fig. 5 to be due to the  $\Delta^{++}$  signal because two combinations are plotted for each event. Thus the requirement of 40% Breit-Wigner implies an 80% contribution of  $\Delta^{++}(1238)p\pi^-$  to the  $pp\pi^+\pi^-$  final state.

Three well-defined enhancements are present in the  $p\pi^-$  mass spectrum [Fig. 6(a)] in the regions of the

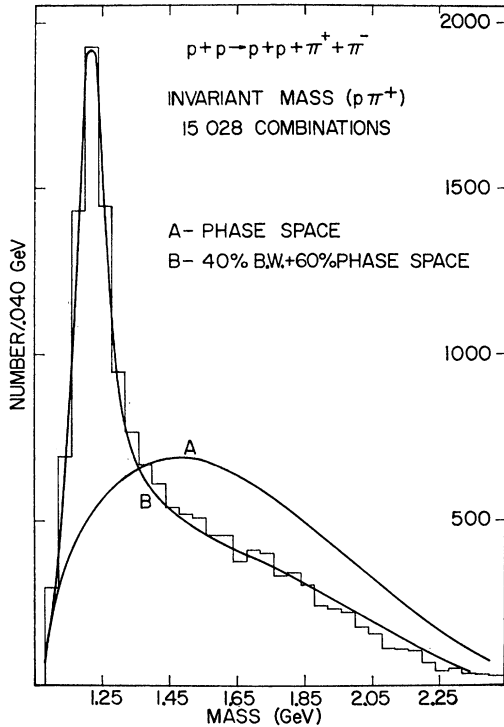


FIG. 5. Spectrum of  $p\bar{p}$  mass in the  $p\bar{p}\pi^+\pi^-$  final state. Two points are plotted for each event. The curve labeled A is the prediction of four-body phase space while the B curve is the prediction of 40% Breit-Wigner [ $\Delta^{++}(1238)$ ] and 60% phase space.

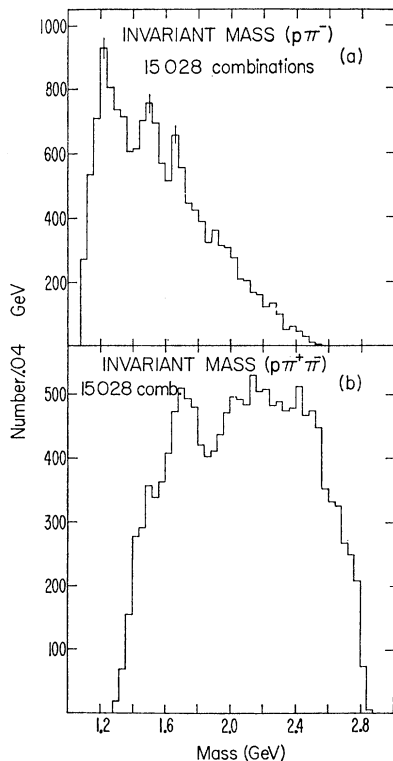


FIG. 6. Invariant-mass spectra in the  $p\bar{p}\pi^+\pi^-$  final state. Two points are plotted for each event. (a)  $M(\pi^+\pi^-)$ ; (b)  $M(p\bar{p})$ .

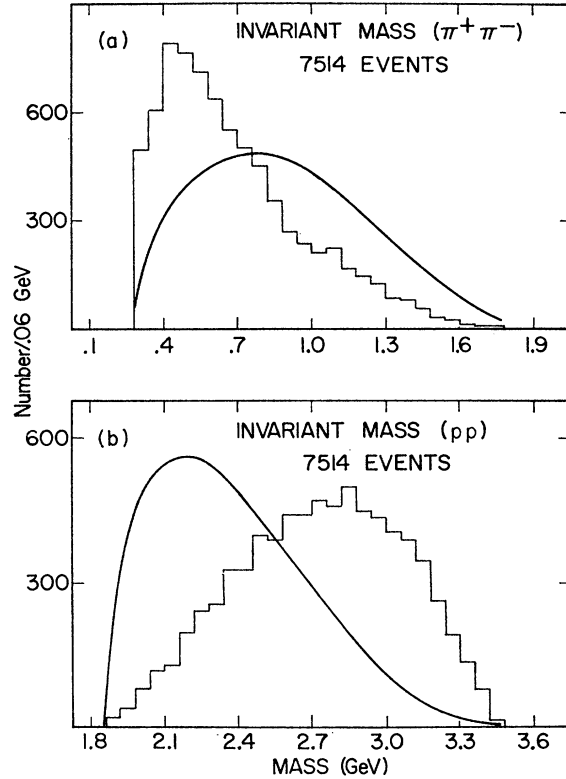


FIG. 7. Invariant-mass spectra in the  $p\bar{p}\pi^+\pi^-$  final state. (a)  $M(\pi^+\pi^-)$ ; (b)  $M(p\bar{p})$ . The curves are predictions of four-body phase space.

well-known  $\Delta^0(1238)$ ,  $N^{*0}(1518)$ , and  $N^{*0}(1688)$  resonances. The  $p\pi^+\pi^-$  spectrum [Fig. 6(b)] displays a slight shoulder at 1500 MeV and a broad enhancement centered near 1700 MeV (FWHM  $\approx 160$  MeV). None of the remaining four distributions (Figs. 7 and 8) have any notable structure. In particular, there is no obvious evidence for  $\rho^0(765)$  meson production in the two-pion mass spectrum [Fig. 7(a)]. However, we show in Sec. VII that if the  $\Delta^{++}(1238)$  events are removed from the sample, a significant  $\rho$  signal remains.

## VI. PROPERTIES OF PERIPHERAL $p\pi\pi$ SYSTEM

### A. $p\pi^+\pi^-$ Mass Spectra

The  $p\pi^+\pi^-$  mass spectra for six ranges of  $t_p$  to the recoiling proton are given in Figs. 9(a)–9(f). These spectra are presented in order to isolate the peripheral components of the enhancement(s) observed in Fig. 6(b) and perhaps to expose new enhancements. An event is plotted twice if both values of  $t_p$  fall within the selected range of  $t_p$ . Contributions to the enhancement seen near 1700 MeV in Fig. 6(b) seem to exist (at least in the form of shoulders) for all  $t_p < 1.0$  GeV<sup>2</sup>. Other peaks are observed in the highly peripheral spectra of Figs. 9(a) and 9(b) near 1450 and 2050 MeV. The cross-hatched events are subject to the additional

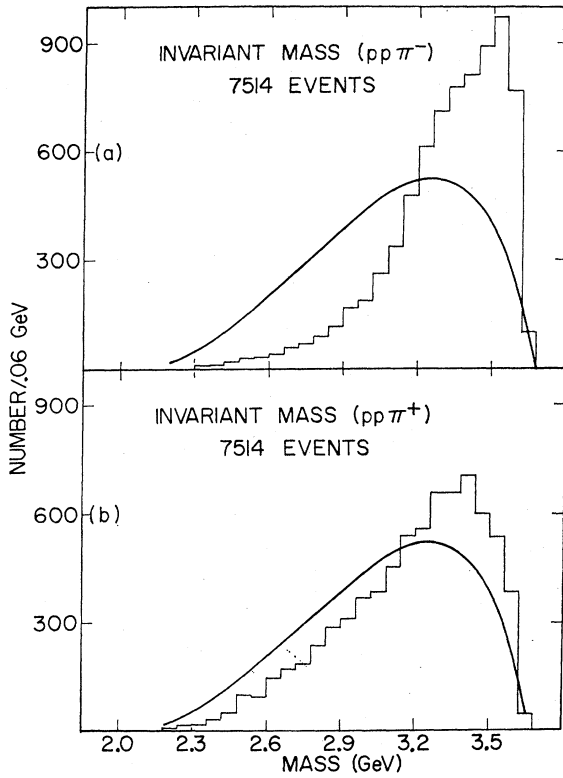


FIG. 8. Invariant-mass spectra in the  $pp\pi^+\pi^-$  final state. (a)  $M(pp\pi^-)$ ; (b)  $M(pp\pi^+)$ . The curves are predictions of four-body phase space.

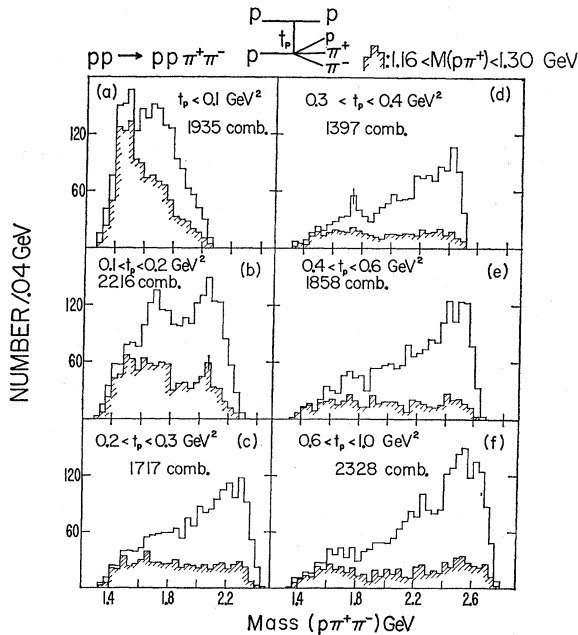


FIG. 9. Distributions of  $\pi^+\pi^-$  mass for the six indicated ranges of  $t$  to the recoiling proton. Both combinations are plotted on one graph if both values of  $t$  simultaneously satisfy the  $t$  selection. The cross-hatched areas represent events with  $1.16 < M(pp\pi^+) < 1.30$  GeV.

restrictions that the  $p\pi^+$  mass be confined to the low-mass  $\Delta^{++}$  region [ $1.16 < M(p\pi^+) < 1.30$  GeV]. The 1450-MeV enhancement seen in Fig. 9(a) is exclusively restricted to events with low  $p\pi^+$  mass. The 2050-MeV peak is also present in the cross-hatched region of Fig. 9(b), thereby suggesting a resonance with a  $\Delta^{++}(1238)\pi^-$  decay mode. The 1700-MeV peak, on the other hand, does not seem to be preferentially linked to  $\Delta^{++}(1238)$  systems. As noted earlier,<sup>9</sup> this result is in disagreement with Alexander *et al.*,<sup>6</sup> who quote a value for the branching ratio

$$\frac{N^{*+}(1700) \rightarrow \Delta^{++}(1238)\pi^-}{N^{*+}(1700) \rightarrow p\pi^+\pi^- (\text{all})} \quad (3)$$

of  $0.74 \pm 0.14$  at 5.5 GeV/c and Almeida *et al.*,<sup>15</sup> who give a ratio of  $0.31 \pm 0.17$  at 10 GeV/c. The different choice of background in the two cases is probably responsible for the difference between the two quoted experimental ratios.

The peripheral 1450-MeV enhancement has also been reported in  $pp \rightarrow pp\pi^+\pi^-$  events for beam momenta ranging from 7.9 to 28.5 GeV/c.<sup>13-21</sup> Early counter experiments<sup>23-25</sup> also detected a bump near 1450 MeV in the peripheral-mass spectra of systems recoiling against a proton in  $pp$  inelastic scattering. In more recent counter experiments other groups<sup>26-28</sup> have observed the same effect for incident beam momenta ranging from 4 to 30 GeV/c. The cross section for the 1450-MeV enhancement seen in counter experiments seems to be rather constant near 0.6 mb. It has been tempting to associate this 1450-MeV enhancement with a  $P_{11}$  resonance at approximately the same mass which has been inferred from phase-shift analyses<sup>29,30</sup> of pion-nucleon scattering. However, the lack of complete information in these counter experiments (angular correlations, etc.) has prevented the assignment of a resonance interpretation to the observed 1450-MeV effect.

The enhancement occurring near 2050 MeV in the  $p\pi^+\pi^-$  and  $\Delta^{++}\pi^-$  mass spectra for  $0.1 < t_p < 0.2$  GeV<sup>2</sup>

<sup>23</sup> G. Cocconi, E. Lillethun, J. P. Scanlon, C. A. Stahlbrandt, C. C. Ting, J. Walters, and A. M. Wetherell, Phys. Letters **8**, 134 (1964).

<sup>24</sup> G. Bellettini, G. Cocconi, A. N. Diddens, E. Lillethun, J. P. Scanlon, A. M. Shapiro, and A. M. Wetherell, Phys. Letters **18**, 167 (1965).

<sup>25</sup> C. M. Ankenbrandt, A. R. Clyde, B. Cork, D. Keefe, L. T. Kerth, W. M. Layson, and W. A. Wenzel, Nuovo Cimento **35**, 1052 (1965).

<sup>26</sup> E. W. Anderson, E. J. Bleser, G. B. Collins, T. Fujii, J. Menes, F. Turkot, R. A. Carrigan, Jr., R. M. Edelstein, N. C. Hien, T. J. McMahon, and I. Nadelhaft, Phys. Rev. Letters **16**, 855 (1966).

<sup>27</sup> I. M. Blair, A. E. Taylor, W. S. Chapman, P. I. P. Kalmus, J. Litt, M. C. Miller, D. B. Scott, H. J. Sherman, A. Astbury, and T. G. Walker, Phys. Rev. Letters **17**, 789 (1966).

<sup>28</sup> K. J. Foley, R. S. Jones, S. J. Lindenbaum, W. A. Love, S. Ozaki, E. D. Platner, C. A. Quarles, and E. H. Willen, Phys. Rev. Letters **19**, 397 (1967).

<sup>29</sup> L. D. Roper, Phys. Rev. Letters **12**, 340 (1964).

<sup>30</sup> P. Baryre, C. Bricman, A. V. Stirling, and G. Villet, Phys. Letters **18**, 342 (1965).

TABLE I. Coefficients in fits of  $e^{bt}$  and  $e^{bt+ct^2}$  to  $dN/dt$  for  $p p \rightarrow (p\pi^+\pi^-)p$  as a function of  $p\pi^+\pi^-$  mass.

Mass range (GeV)	$t$ bin range (GeV <sup>2</sup> )	No. of points	Fits to $e^{bt}$		Fits to $e^{bt+ct^2}$		
			$\chi^2$ of fit	$b$ (GeV <sup>-2</sup> )	$\chi^2$ of fit	$b$ (GeV <sup>-2</sup> )	$c$ (GeV <sup>-4</sup> )
1.22-1.5	0-0.4	10	15.1	-8.8±0.4	5.0	-12.6±1.3	11.6±3.6
1.5-1.6	0-0.6	15	33.4	-6.1±0.3	9.5	-10.2±0.9	8.1±1.7
1.6-1.7	0-0.6	15	17.4	-6.1±0.3	13.6	-7.7±0.9	3.4±1.7
1.7-1.8	0-0.8	20	30.0	-4.8±0.2	18.4	-6.8±0.6	3.0±0.9
1.8-1.9	0.04-0.8	19	37.5	-4.6±0.2	25.2	-7.0±0.7	3.6±1.0
1.9-2.0	0.04-1.0	24	48.4	-3.4±0.1	25.9	-5.9±0.5	2.7±0.6
2.0-2.1	0.08-1.0	23	25.0	-3.8±0.2	10.6	-6.0±0.6	2.4±0.6
2.1-2.2	0.08-1.2	28	51.5	-3.0±0.1	31.8	-5.1±0.5	1.9±0.4
2.2-2.3	0.12-1.4	32	67.0	-2.6±0.1	46.9	-4.5±0.4	1.4±0.3
2.3-2.4	0.16-1.4	31	75.8	-2.2±0.1	30.1	-5.5±0.5	2.2±0.3
2.4-2.5	0.24-1.4	29	34.7	-1.9±0.1	23.3	-3.9±0.6	1.3±0.4
2.5-2.6	0.36-1.6	31	29.6	-1.7±0.1	25.0	-3.0±0.6	0.7±0.3

is approximately a 3-standard-deviation effect. The Cambridge group<sup>16</sup> has also seen the same effect in their peripheral  $p\pi^+\pi^-$  mass spectrum at 16 GeV/c. Presently the only known resonances in this region are the  $\Delta^+(1950)$  and  $N^{*+}(2190)$  and a  $D_{13}$  state of mass and width 2060 and 290 MeV which has been reported by the CERN group.<sup>31</sup> In addition, Yoon *et al.*<sup>32</sup> report a very narrow enhancement ( $M, \Gamma=2080, 40$ ) seen in the reaction  $\pi^- p \rightarrow \pi^- p \pi^+ \pi^- \pi^0$ . They observed the effect via a  $\Delta(1238)\rho(765)$  decay mode.

The enhancement appearing in the  $p\pi^+\pi^-$  mass spectrum [Fig. 6(b)] in the region of 1700 MeV has been observed at other beam momenta from 4.0 to 28.5 GeV/c.<sup>4-8,13-21</sup> It accounts for no more than 10% of the over-all sample in this experiment. This percentage is consistent with the values of 8% reported at 4.0<sup>4</sup> and 6.0 GeV/c,<sup>7</sup> and 9% which is quoted at 10.0 GeV/c.<sup>15</sup> Thus the cross section for  $N^{*+}(1700)$  production seen in  $p p \rightarrow p\pi^+\pi^-$  final states is no more than 0.25 mb in the intermediate energy range. As mentioned above, the  $t$  dependence for this state can be described by a more gradually decreasing function than for the highly peripheral events occurring in the " $N^*(1450)$ " region. Presumably this is the same 1700-MeV effect that has been observed in counter experiments<sup>23-28</sup> with beam momenta from 4 to 30 GeV/c. A relatively constant production cross section of approximately 0.55 mb is observed for the reaction  $p p \rightarrow p N^{*+}(1700)$  over the entire quoted range of beam energies. Although it is generally accepted that a resonance or several resonances give rise to the observed 1700-MeV enhancements, the large and generally unknown character of the background has thus far prevented any detailed investigation of the production mechanisms or of the dominant partial-wave structure.

## B. Momentum Transfer Distribution to $p\pi^+\pi^-$ System

The distributions in momentum transfer to the  $p\pi^+\pi^-$  system have been fitted to the functions  $e^{bt+ct^2}$

<sup>31</sup> A. Donnachie, R. G. Kirsopp, and C. Lovelace, CERN Report No. 67/1283/5-Th. 838 (unpublished).

<sup>32</sup> T. S. Yoon, P. Berenyi, A. W. Key, J. D. Prentice, N. R. Stenberg, and W. D. Walker, Phys. Letters **24B**, 307 (1967).

and  $e^{bt}$  for different selections on  $p\pi^+\pi^-$  effective mass. The results of these fits are given in Table I. In these fits, a  $p\pi^+\pi^-$  mass combination is used if its momentum transfer falls within the  $t$  range noted in Table I for the mass selection being considered. The momentum transfer used is calculated with respect to the initial-state proton traveling in the same c.m. hemisphere as the outgoing  $p\pi^+\pi^-$  system.

The linear coefficient  $b$ , obtained in the quadratic fits of Table I, is plotted versus  $p\pi^+\pi^-$  mass in Fig. 10.  $-b$  is seen to decrease in a rather striking manner from a value of  $\sim 12$  GeV<sup>-2</sup> at threshold to a value of  $\sim 3$  GeV<sup>-2</sup> at  $M(p\pi\pi) \sim 2.5$  GeV. This well-known effect characterizes the sharp  $t$  dependences of diffraction-produced systems whose production is most significant for low-mass systems. Alternatively, the effect may also be qualitatively understood in terms of a one-pion-exchange (OPE) picture in which the diffractive component at the  $\pi^- p$  vertex contributes dominantly to the low ( $p\pi^+\pi^-$ ) mass peak (Deck effect). Whether

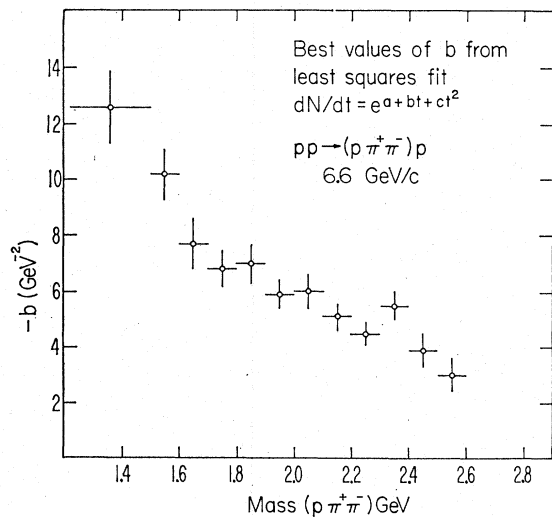


FIG. 10. Mass dependence of the coefficient  $b$ , obtained in least-squares fits of the  $p\pi^+\pi^-$   $dN/dt$  distributions to the forms  $e^{bt+ct^2}$ .  $t$  is the momentum transfer to the  $p\pi^+\pi^-$  system.

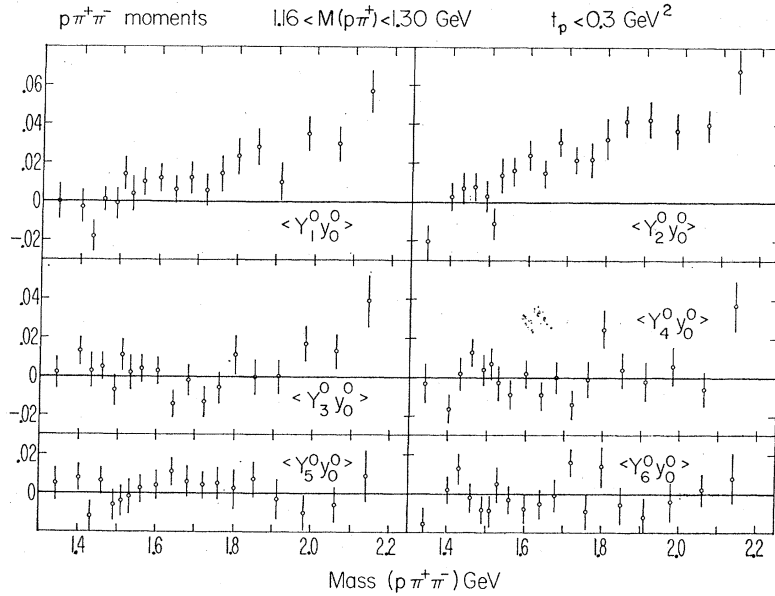


FIG. 11. Experimental uncorrelated  $\langle Y_L^0 y_0^0 \rangle$  moments of the peripheral  $\Delta^{++}\pi^-$  system as a function of mass of the  $\Delta^{++}\pi^-$  system for  $L=1-6$ . The argument of the spherical harmonic function is a unit vector along the direction of the  $\Delta^{++}$  in the  $\Delta^{++}\pi^-$  rest frame (Ref. 33) [see Eq. (5)].

the elementary Deck model or a more elaborate version in which there is a final-state interaction between the ( $p\pi^+$ ) and  $\pi^-$  systems accounts for the observation, one expects (on kinematic grounds) the  $t$  dependence of the  $p\pi^+\pi^-$  system to be sharper for events in the low  $p\pi^+\pi^-$  mass "Deck region." This model is discussed in more detail in Sec. VIII.

### C. Angular Correlations in $p\pi^+\pi^-$ System

As a means of examining in more detail possible structure in the  $p\pi^+\pi^-$  system, we have studied various angular correlations as a function of the effective mass of the system. In order to most easily study the complete angular correlations of the system, we consider the process as a quasi-two-body reaction

$$\begin{aligned} p p &\rightarrow (\Delta^{++}\pi^-) p \\ (\Delta^{++}\pi^-) &\rightarrow \Delta^{++}\pi^- \\ \Delta^{++} &\rightarrow p\pi^+. \end{aligned} \quad (4)$$

The  $\Delta^{++}$  cut used is  $1.16 < M(p\pi^+) < 1.3$  GeV. The correlation moment

$$\langle Y_L^M y_l^m \rangle = \frac{1}{N} \sum_{i=1}^N Y_L^M(\hat{\Delta}_{\Delta\pi_i}) y_l^m(\hat{p}_{\Delta_i}) \quad (5)$$

is evaluated for the  $N$  events in a particular ( $\Delta^{++}\pi^-$ ) mass bin with  $t < 0.3$  GeV<sup>2</sup>. As indicated in Eq. (5), the arguments of the spherical harmonic functions are unit vectors along the direction of the  $\Delta^{++}$  in the  $\Delta^{++}\pi^-$  rest frame and the proton in the  $\Delta^{++}$  rest frame. The coordinate system used for both vectors is the conventional  $t$ -channel system.<sup>33</sup>

<sup>33</sup> In the conventional  $t$ -channel system, the incident proton, as seen in the  $\Delta^{++}\pi^-$  rest frame, is taken as the polar axis; the  $y$  axis is along the normal to the production plane.  $\hat{y} = \hat{n} \sim \hat{p}_p \times \hat{p}_{\Delta^{++}\pi^-}$ .

The uncorrelated  $\langle Y_L^0 y_0^0 \rangle$  and correlated  $\langle Y_L^0 y_2^0 \rangle$  moments are displayed in Figs. 11 and 12, respectively. In Fig. 11, the  $\langle Y_1^0 y_0^0 \rangle$  and  $\langle Y_2^0 y_0^0 \rangle$  moments become

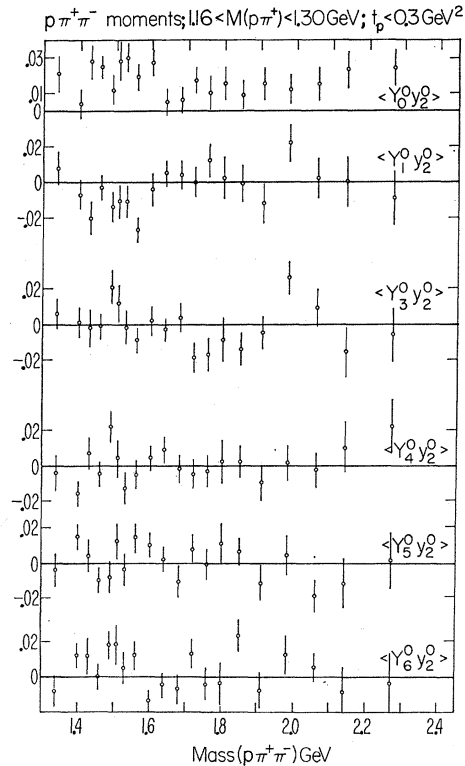


FIG. 12. Experimental correlated  $\langle Y_L^0 y_2^0 \rangle$  moments of the peripheral  $\Delta^{++}\pi^-$  system as a function of mass of the  $\Delta^{++}\pi^-$  system. The arguments of the spherical harmonic functions are unit vectors along the direction of the  $\Delta^{++}$  in the  $\Delta^{++}\pi^-$  rest frame and the proton in the  $\Delta^{++}$  rest frame (Ref. 33) [see Eq. (5)].



increasingly more positive at larger mass, indicating that at low mass the  $\Delta^{++}\pi^-$  system is dominantly  $s$  wave while  $p$  wave becomes increasingly more important as one goes up to larger mass. There are indications of structure for  $L=3-6$ , but clearly an order of magnitude increase in statistics is necessary to determine the structure.

The correlation moments in Fig. 12 also indicate structure as a function of  $\Delta^{++}\pi^-$  mass which a higher-statistics experiment would reveal more clearly. Several points may tentatively be noted, such as the observation that  $\langle Y_1^0 y_2^0 \rangle$  seems significantly negative in the 1.5-GeV mass region and that some structure in the higher- $l$  moments in the 1.5-GeV mass region may be present. The  $\langle Y_2^0 y_2^0 \rangle$  moment is not shown in Fig. 12, but rather in Fig. 13, together with two other correlation moments which have a particular interest as discussed in Sec. VI D.

Higher statistics are clearly necessary in order to draw definitive conclusions. The point to be made here is that structure in these moments complements the information seen in the  $\Delta^{++}\pi^-$  mass spectrum and, as such, these moment quantities deserve serious consideration in future analyses of higher-statistics samples. They represent natural parameters for analysis of data of this type in a picture where a beam proton under-

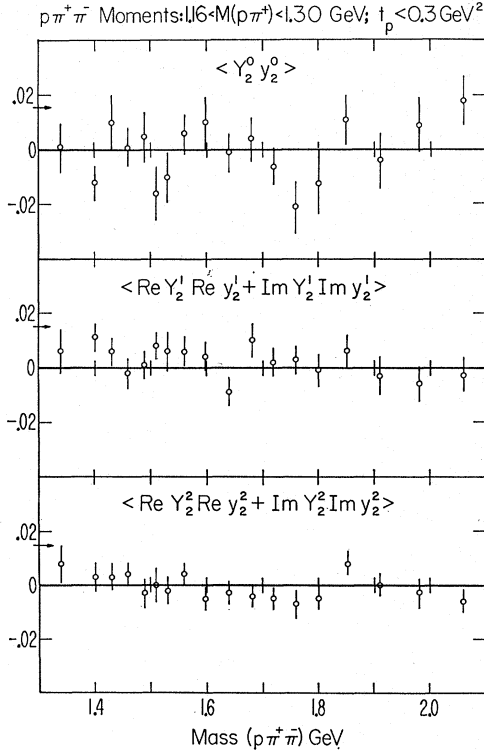


FIG. 13. Distributions of the correlated moments which are expected to be nonzero for  $P_{11}$  production of the  $\Delta^{++}\pi^-$  system ( $J^P = \frac{1}{2}^+ \Delta^{++}\pi^-$ ) and subsequent decay of the  $J^P = \frac{3}{2}^+ \Delta^{++}$  into a proton and  $\pi^+$ . The arrows at the left-hand side indicate the expected values.

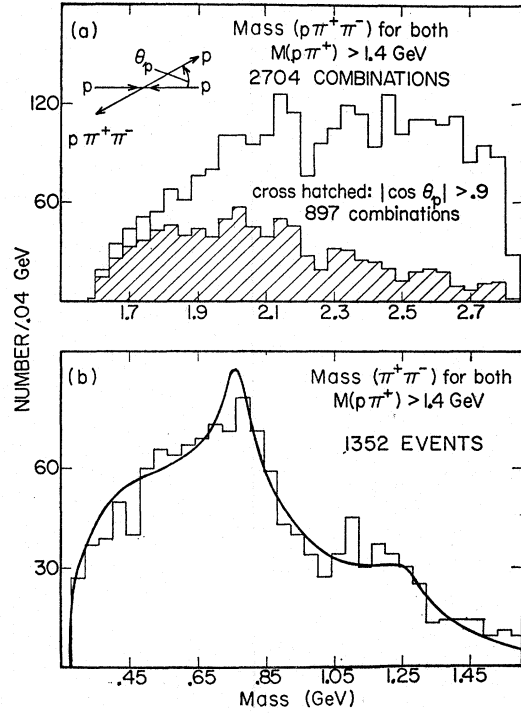


FIG. 14. Invariant-mass spectra for the 1352 events with both  $p\pi^+$  masses greater than 1.4 GeV. (a)  $M(p\pi^+\pi^-)$ : Two combinations are plotted for each event. The events represented by the cross-hatched area have  $|\cos \theta_p| > 0.9$ . (b)  $M(\pi^+\pi^-)$ : The solid curve is the Monte Carlo prediction assuming a cubic background and Breit-Wigner distribution (in the square of the matrix element) for the  $\rho^0$  and  $f^0$  resonances (see Sec. VII).

goes diffraction scattering, turning into a  $\Delta^{++}\pi^-$  system whose angular momentum composition depends on  $\Delta^{++}\pi^-$  mass.

#### D. Angular Correlation Investigation of $P_{11} \rightarrow \Delta^{++}\pi^-$ Breakup

The question of whether the low-mass  $\Delta^{++}\pi^-$  mass peak represents dominant production of the  $P_{11}$  Roper resonance, as has been believed by some people, can be partially answered by examination of the angular correlation situation.

For a  $J^P = \frac{1}{2}^+ \rightarrow \Delta^{++}\pi^-$  state, the joint angular distribution of the  $\hat{\Delta}_{\Delta\pi}$  and  $\hat{p}_{\Delta}$  unit vectors, discussed in Sec. VI C, can be shown to have the form

$$D(\hat{\Delta}_{\Delta\pi}, \hat{p}_{\Delta}) = \frac{1}{4\pi} Y_0^0 y_0^0 + \frac{1}{20\pi} Y_2^0 y_2^0 + \frac{1}{10\pi} [\text{Re}(Y_2^1) \text{Re}(y_2^1) + \text{Im}(Y_2^1) \text{Im}(y_2^1)] + \frac{1}{10\pi} [\text{Re}(Y_2^2) \text{Re}(y_2^2) + \text{Im}(Y_2^2) \text{Im}(y_2^2)]. \quad (6)$$

TABLE II. Results of fits to the  $M(\pi^+\pi^-)$  distribution for the cut data [both  $M(p\pi^+) > 1.4$  GeV].

Background type	Confidence level (%)	$\sigma$ ( $\mu\text{b}$ )	$\rho^0$ Mass (GeV)	Width (GeV)	$\sigma$ ( $\mu\text{b}$ )	$f^0$ Mass (GeV)	Width (GeV)
Quadratic	29	$94 \pm 19$	0.765 <sup>a</sup>	0.125 <sup>a</sup>	$32 \pm 12$	1.264 <sup>a</sup>	0.151 <sup>a</sup>
Cubic	24	$99 \pm 21$	0.765 <sup>a</sup>	0.125 <sup>a</sup>	$30 \pm 14$	1.264 <sup>a</sup>	0.151 <sup>a</sup>
Quadratic	21	$76 \pm 24$	$0.771 \pm 0.011$	$0.091 \pm 0.038$	$22 \pm 11$	$1.247 \pm 0.013$	$0.065 \pm 0.041$
Cubic	17	$85 \pm 31$	$0.771 \pm 0.019$	$0.100 \pm 0.044$	$20 \pm 10$	$1.247 \pm 0.013$	$0.060 \pm 0.040$

<sup>a</sup> Fixed values.

The expected values of the three  $l \neq 0$  moments of  $\sim 0.016$ ,  $\sim 0.016$ , and  $\sim 0.016$ , respectively, are shown by arrows in Fig. 13 together with the experimental values of these moments. Although the  $\langle Y_2^0 Y_2^0 \rangle$  moment is not incompatible with the expected value in the region of  $\sim 1450$  MeV, the other two  $m \neq 0$  moments seem not to be compatible with expectation in this region. It thus appears that the  $\Delta^{++}\pi^-$  system does not have the angular correlation properties expected for a pure  $P_{11}$  system. This, of course, does not exclude the presence of a  $P_{11}$  component in the  $\sim 1450$  enhancement; it simply suggests that this enhancement is not dominated by production of the  $P_{11}$  resonance.

### VII. EVENTS WITHOUT $\Delta^{++}(1238)$ PRODUCTION

This section is included for the purpose of examining the  $\pi\pi$  mass spectrum for  $\rho^0(765)$  production and the  $p\pi\pi$  spectrum for high-mass inelastic  $N^{*+}$  resonances (possibly not peripherally produced) when an attempt is made to exclude the  $\Delta^{++}$  events.

In order to select a sample of events relatively free of  $\Delta^{++}$  background, events were chosen only if both  $p\pi^+$  masses were greater than 1.40 GeV. 1352 events satisfied this restriction. Several effective-mass spectra were plotted for these 1352 events. No enhancements were observed in the remaining  $p\pi^+$  or  $p\pi^-$  spectra. Therefore, the resonances observed in Fig. 6(a) prefer to be produced with corresponding  $\Delta^{++}$  systems. The  $M(p\pi^+\pi^-)$  spectrum is given in Fig. 14(a). The cross-hatched events are those with a peripheral c.m. cosine selection ( $|\cos\theta_p| > 0.9$ ); no significant enhancements are evident. The corresponding  $M(\pi^+\pi^-)$  spectrum is displayed in Fig. 14(b). Both  $\rho^0(765)$  and  $f^0(1260)$  production seem to occur. Most of the  $\rho^0$  events occur with  $M(p\pi^+\pi^-) > 2.0$  GeV. In addition, the protons produced in the  $\rho^0$  events do not appear to simultaneously have small values of momentum transfer with respect to the incident protons.

Maximum-likelihood fits of the theoretical differential cross section to the corresponding experimental data have been performed upon the selected sample of 1352 events. The absolute square of the matrix element (in the formula) was taken to be quadratic or cubic in  $M(\pi^+\pi^-)$ . The fits yielded confidence levels near 1%.

In addition, the data at the  $\rho^0$  and  $f^0$  positions [in the  $M(\pi^+\pi^-)$  spectrum] exceeded the best-fit quadratic and cubic predictions by roughly 3.5 and 1.5 standard deviations, respectively. A better description of the data in Fig. 14(b) has been obtained by adding to the above matrix element an incoherent sum of two Breit-Wigner distributions (with the masses and widths of the  $\rho^0$  and  $f^0$ ). In each case maximum-likelihood fits were attempted using both fixed and free values for the resonance parameters. The results of the fits (including the masses and widths of the  $\rho^0$  and  $f^0$ ) are present in Table II. The cross sections listed in Table II have been corrected for the  $\rho^0$  and  $f^0$  events removed by the  $\Delta^{++}$  mass cut: This is done by generating Monte Carlo events subject to four-body phase space modified by the matrix element [which depends upon  $M(\pi^+\pi^-)$ ]; the cross sections from the fits are then divided by the fraction of  $pp \rightarrow pp\rho^0$  or  $pp \rightarrow pp f^0$  Monte Carlo events with both  $p\pi^+$  masses exceeding 1.4 GeV to give the final result. The solid curve drawn in Fig. 14(b) is the Monte Carlo prediction for the  $M(\pi^+\pi^-)$  spectrum assuming a cubic background and Breit-Wigner distributions for the  $\rho^0$  and  $f^0$  resonances in the absolute square of the matrix element. The resonance param-

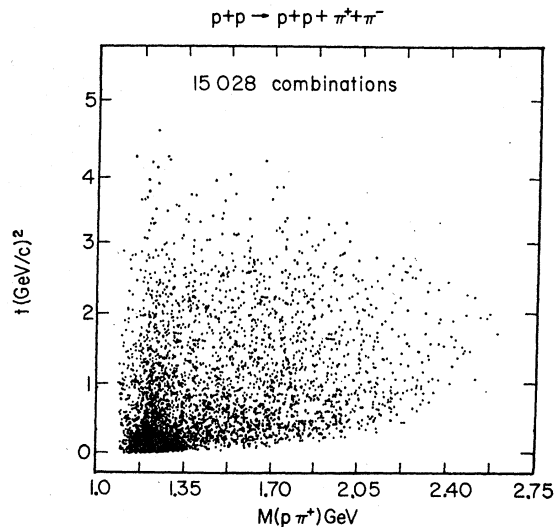
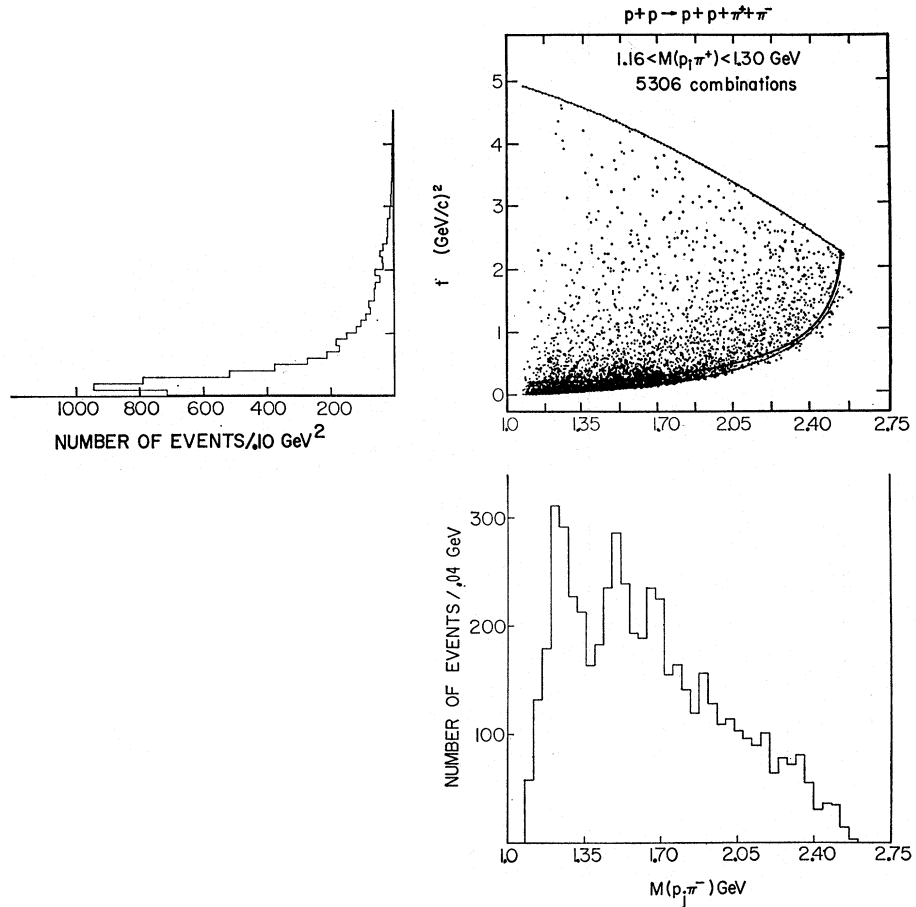


FIG. 15. Scatter plot of  $p\pi^+$  mass vs  $t$  for the 7514  $pp\pi^+\pi^-$  events. Two points are plotted for each event.

FIG. 16. Chew-Low scatter plot of  $M(p_j \pi^-)$  vs  $t$  for events with  $1.16 < M(p_i \pi^+) < 1.30$  GeV (692 events are plotted twice). The interior smooth curve is the line of  $|\cos \theta_{\Delta^{++}}^{c.m.}| = 0.965$  drawn for the central  $\Delta^{++}$  value of  $M(p_i \pi^+) = 1.23$  GeV. The projections of  $M(p_j \pi^-)$  and  $t$  are also given.



eters and cross sections used in the Monte Carlo calculation are those of the second fit listed in Table II. The curve and the data agree quite well in Fig. 14(b).

Averaging the cross sections for the first two fits listed in Table II (those fits using fixed masses and widths) we obtain  $\sigma_{\rho^0} = 97 \pm 20 \mu\text{b}$  and  $\sigma_{f^0} = 31 \pm 13 \mu\text{b}$ . The  $pp\rho^0$  cross section is in agreement with Alexander *et al.*,<sup>6</sup> who quote a value of  $70 \pm 50 \mu\text{b}$  at 5.5 GeV/c, and with Yekutieli *et al.*,<sup>6</sup> who obtained values for  $\sigma_{\rho^0}$  from  $90 \pm 30 \mu\text{b}$  to  $130 \pm 40 \mu\text{b}$  (depending upon the chosen background) at 6.92 GeV/c. Our  $pp\rho^0$  cross section disagrees with the upper limit of  $50 \mu\text{b}$  obtained by Caso *et al.*<sup>7</sup> at 6.0 GeV/c. It must be pointed out that our analysis, as well as that of Yekutieli *et al.*,<sup>6</sup> is based upon data with restricted ranges of  $p\pi^+$  mass whereas the analyses at 5.5 and 6.0 GeV/c are based on the entire samples of  $pp\pi^+\pi^-$  data (which poses a large-background problem).

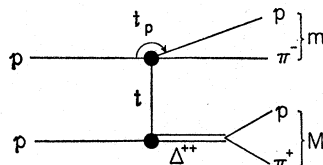


FIG. 17. One-pion-exchange process for  $pp \rightarrow \Delta^{++} p \pi^-$ .

### VIII. $\Delta^{++} p \pi^-$ PRODUCTION

Figure 5 indicates that  $\sim 80\%$  of the  $pp\pi^+\pi^-$  events involve  $\Delta^{++}(1238)$  production. The majority of  $\Delta^{++}$  systems are produced very peripherally. In order to illustrate this point, we show in Fig. 15 a two-dimensional scatter plot of the  $p\pi^+$  mass versus the lower of the two possible momentum transfers  $t$  from the beam or target proton to the outgoing  $p\pi^+$  system. Two points are plotted for each event.

The corresponding Chew-Low plot of  $p\pi^-$  mass versus  $t$  is plotted in Fig. 16 for the  $\Delta^{++} p \pi^-$  events. An event is called  $\Delta^{++} p \pi^-$  if  $1.16 < M(p\pi^+) < 1.30$  GeV. Both  $p\pi^-$  mass combinations are plotted if both of the corresponding  $p\pi^+$  mass combinations fall within the  $\Delta^{++}$  band.<sup>34</sup> Most of the peripheral events occur below the solid curve which is the line of  $|\cos \theta_{\Delta^{++}}^{c.m.}| > 0.965$ .  $\theta_{\Delta^{++}}^{c.m.}$  is the c.m. angle between the incoming beam proton and the outgoing  $\Delta^{++}$ . The line is calculated for a central  $\Delta^{++}$  mass value of 1.230 GeV. The projections of  $p\pi^-$  mass and  $t$  are also shown in Fig. 16. The features evident in the  $M(p\pi^-)$  projection are the continued presence of three well-defined peaks in the

<sup>34</sup> This occurs for 692 of the 4614 events plotted.

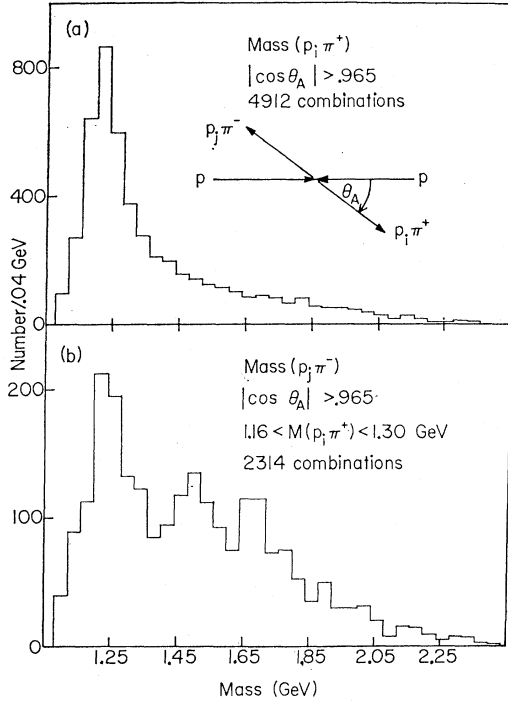


FIG. 18. (a) Distribution of  $p\pi^+$  mass for combinations with  $|\cos\theta_{p\pi^+c.m.}| > 0.965$ . (b) Distribution of  $p\pi^-$  mass for the 2314  $\Delta^{++}p\pi^-$  combinations with the same peripheral selection as in (a).

regions of the  $\Delta^0(1238)$ ,  $N^{*0}(1518)$ , and  $N^{*0}(1688)$  resonances. There are no statistically significant enhancements for  $M(p\pi^-) > 1700$  MeV.

The peripheral nature of the  $pp \rightarrow \Delta^{++}\pi^-p$  reaction and in particular of the quasi-two-body processes  $pp \rightarrow \Delta^{++}\Delta^0$  and  $\Delta^{++}N^{*0}$  invites further analysis of the data in terms of the exchange process depicted in Fig. 17. We first study the angular distribution of the outgoing protons in their respective vertex c.m. systems and show that these angular distributions are very similar to those of on-mass-shell  $\pi^\pm p$  scattering, as reported earlier for a preliminary sample of data.<sup>9</sup> We then compare the shape and magnitude of the experimental distributions in the Chew-Low plane with the absolute predictions of OPE phenomenology.<sup>11</sup> Next we study the  $m_{\Delta\pi}$  distribution in the light of these results and un-Reggeized and Reggeized Deck-model calculations, the latter of which were reported earlier in preliminary form in collaboration with Berger.<sup>10</sup> We defer discussion of the  $\phi$  or Treiman-Yang angular distribution in the  $\pi^-p$  system to these sections because of the intimate kinematic relationship between  $m_{\Delta\pi}$  and  $\phi$ . Finally, to complete the picture, we compare the  $\Delta^{++}\pi^-p$  final state with the final states  $\Delta^{++}\pi^-p\pi^0$  and  $\Delta^{++}\pi^-n\pi^+$  to demonstrate that the latter two final states seem to result from the scattering of a proton on a virtual  $\pi^-$  resulting in the inelastic reactions  $\pi^-p \rightarrow \pi^-p\pi^0$ ,  $\pi^-n\pi^+$ .<sup>12</sup>

For the remainder of this section we use the symbols

shown in Fig. 17, in which  $m$  represents the  $\pi^-p$  effective mass and  $M$  the  $\pi^+p$  effective mass.

### A. Angular Distributions in $\pi^-p$ and $\pi^+p$ Rest Frames

In order to restrict the analysis to peripheral events and to effectively remove background contamination due to "wrong  $p\pi^+$ " mass combinations, we use only events with  $|\cos\theta_{p\pi^+c.m.}| > 0.965$ . The  $p\pi^+$  mass spectrum is exhibited in Fig. 18(a). At the central position of the  $\Delta^{++}$  we estimate that the nonresonant background level is  $\leq 10\%$  of the peak value. Figure 18(b) shows the  $p\pi^-$  mass spectrum for the peripheral  $\Delta^{++}p\pi^-$  events. This sample consists of 2130 events, of which 184 have both  $\Delta^{++}$  combinations with  $|\cos\theta_{\Delta^{++}c.m.}| > 0.965$  and are plotted twice.

For the purpose of studying the quasi-elastic  $\pi^-p$  scattering, these 2130 events are divided into 19  $p\pi^-$  mass intervals and the  $\pi^-p$  c.m. angular distribution in each of these intervals is studied separately. The scattering angle  $\theta$  is the angle between the incoming and outgoing protons at the  $p\pi^-$  vertex as seen in the  $p\pi^-$  rest frame.  $\cos\theta$  is related to the two momentum transfers in Fig. 17 via the equations

$$\cos\theta = \frac{2E_{in}E_{out} - 2m_p^2 - t_p}{2|\mathbf{P}_{in}||\mathbf{P}_{out}|}, \quad (7)$$

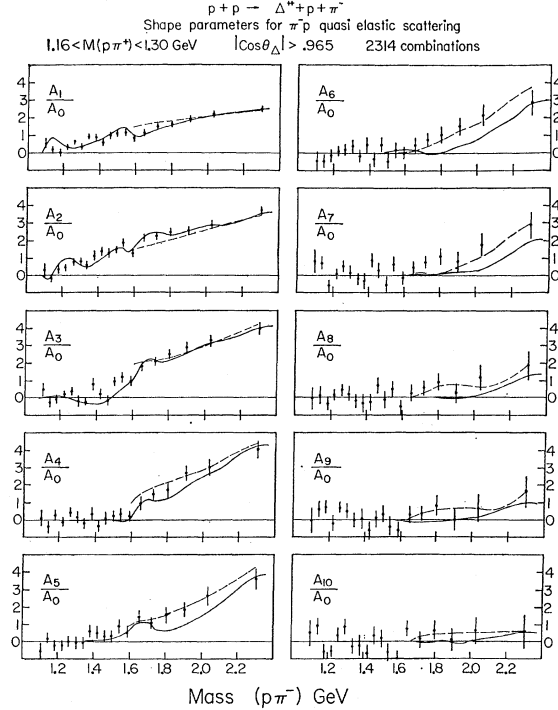


FIG. 19.  $A_L/A_0$  shape parameters [as defined by Eq. (11)] of the  $p\pi^-$  quasi-elastic scattering distribution as a function of  $p\pi^-$  mass. The moments are calculated only for the 2314  $\Delta^{++}p\pi^-$  combinations with  $|\cos\theta_{\Delta}| > 0.965$ . The solid curves were derived from the known  $\pi N$  phase shifts as determined in real  $\pi N$  scattering experiments. The dashed curves are the predictions of a Reggeized pion-exchange model which is described in Sec. VIII E.

where

$$|\mathbf{P}_{\text{in}}| = \frac{1}{2m} \{ [(m-m_p)^2 + t] [(m+m_p)^2 + t] \}^{1/2} \quad (8)$$

and

$$|\mathbf{P}_{\text{out}}| = \frac{1}{2m} \{ [(m-m_p)^2 - \mu^2] [(m+m_p)^2 - \mu^2] \}^{1/2}. \quad (9)$$

Using the conventional Legendre polynomials expansion of the differential cross section,

$$\frac{d\sigma}{d\Omega} = \lambda^2 \sum A_L P_L(\cos\theta) = \frac{\sigma}{4\pi} \sum \left( \frac{A_L}{A_0} \right) P_L(\cos\theta), \quad (10)$$

the "shape parameters" ( $A_L/A_0$ ) of the angular distribution are determined by evaluating for each  $L$  the average value of the Legendre polynomial  $P_L(\cos\theta)$  over the events in the sample:

$$A_L/A_0 = (2L+1) \langle P_L(\cos\theta) \rangle. \quad (11)$$

The statistical uncertainty is given by

$$\delta \left( \frac{A_L}{A_0} \right) = \frac{(2L+1)}{\sqrt{N}} [ \langle P_L^2 \rangle - \langle P_L \rangle^2 ]^{1/2}, \quad (12)$$

where  $N$  is the total number of events in the  $p\pi^-$  mass interval.

The  $A_L/A_0$  shape parameters (or moments) of the  $p\pi^-$  quasi-elastic scattering for  $L=1$  through  $L=10$  are shown in Fig. 19 as a function of the  $p\pi^-$  mass. The solid curves which appear in Fig. 19 were derived from existing real  $p\pi^-$  elastic-scattering data; the curves were drawn through points calculated from the phase shifts of Roper *et al.*<sup>35</sup> below 1.6 GeV, and from the results of Duke *et al.*<sup>36</sup> and Hill *et al.*<sup>37</sup> for  $p\pi^-$  masses greater than 1.6 GeV. The agreement between the data and the curves in Fig. 19 is reasonably good below 1.7 GeV for all of the moments. Above 1.7 GeV the higher ( $L \geq 4$ ) moments tend to exceed the curves somewhat. This corresponds to an apparent sharpening of the angular distribution for high  $p\pi^-$  masses, which is shown below to be related to the low-mass  $\Delta^{++}\pi^-(1450)$  enhancement. The dashed curves in Fig. 19 are the predictions of a Reggeized Deck model which is described in Sec. VIII E.

The corresponding  $A_L/A_0$  for the  $p\pi^+$  vertex are shown<sup>38</sup> in Fig. 20. The moments are given for  $M(p\pi^+) < 1.5$  GeV only. The data agree reasonably well with the free  $p\pi^+$  scattering results in the region  $\sim 1.25$ -1.35

<sup>35</sup> L. D. Roper, R. M. Wright, and B. T. Feld, Phys. Rev. **138**, B190 (1965).

<sup>36</sup> P. J. Duke, D. P. Jones, M. A. R. Kemp, P. G. Murphy, J. D. Prentice, J. J. Thresher, H. H. Atkinson, C. R. Cox, and K. S. Heard, Phys. Rev. Letters **15**, 468 (1965).

<sup>37</sup> R. E. Hill, N. E. Booth, R. J. Esterling, S. Suwa, and A. Yokosawa, Phys. Rev. D **1**, 729 (1970).

<sup>38</sup> The  $A_L/A_0$  moments for  $L$  values higher than 3 have also been evaluated and are consistent with zero up to  $M=1.5$  GeV, in agreement with real  $p\pi^+$  scattering experiments.

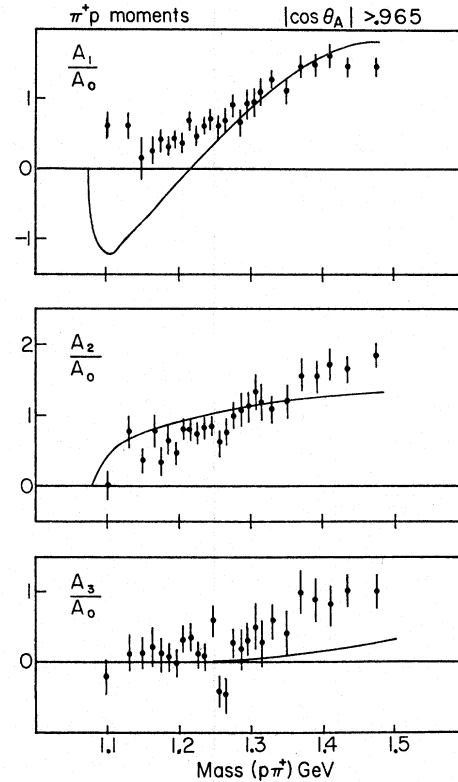


FIG. 20.  $A_L/A_0$  shape parameters [as defined by Eq. (11)] of the  $p\pi^+$  quasi-elastic scattering distribution as a function of  $p\pi^+$  mass. The moments are calculated for combinations with  $|\cos\theta_{p\pi^+c.m.}| > 0.965$ . The solid curves were derived from the known  $\pi N$  phase shifts as determined in real  $\pi N$  scattering experiments.

GeV. The disagreement in the  $A_1/A_0$  moment below 1.3 GeV is most likely due to the off-mass-shell behavior<sup>39,40</sup> of the  $\pi^+p$  scattering. Colton and Schlein<sup>39</sup> have pointed out that this effect is a characteristic of low-momentum-transfer  $p\pi^+$  systems, whether produced by  $\pi$ ,  $K$ , or proton beams.

We observe reasonably good agreement between the  $\pi^-p$  quasielastic scattering moments for a wide range of  $\pi^-p$  mass, the  $\pi^+p$  moments in the  $\Delta^{++}$  region, and those corresponding moments determined from real  $\pi^\pm p$  scattering data. Therefore, we proceed with the assumption that the process shown in Fig. 17 dominates the production of the peripheral  $\Delta^{++}p\pi^-$  state.

## B. Chew-Low Distribution

We now present a study of the low-momentum-transfer component of the Chew-Low distribution

<sup>39</sup> Eugene Colton and Peter E. Schlein, in *Proceedings of the Conference on  $\pi\pi$  and  $K\pi$  Interactions* (Argonne National Laboratory, Argonne, Ill., 1969), p. 1.

<sup>40</sup> The disagreement in  $A_1/A_0$  for  $M < 1.25$  GeV is not due to wrong combination assignments because it is also seen in the reaction  $pp \rightarrow p\pi^+n$  at 6.6 GeV/c, where there is just one  $M$  combination. In addition, as demonstrated in Ref. 39, the same effect is also observed in the reactions  $K^+p \rightarrow (\pi^+p)K^+\pi^-$  and  $\pi^+p \rightarrow (\pi^+p)\pi^+\pi^-$ .

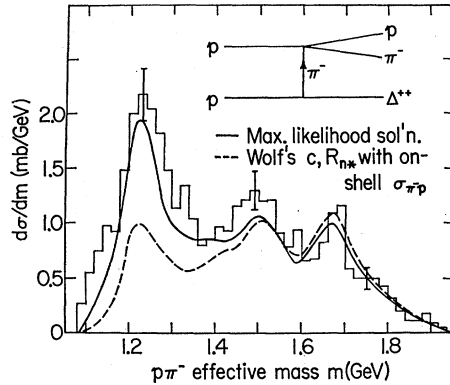


FIG. 21. Differential cross section for  $p\pi^-$  effective mass ( $m$ ) for the  $t$  and  $\Delta^{++}$  selections quoted in Eqs. (13). The curves are discussed in Sec. VIII B. The inset represents the OPE process considered in the analysis.

shown in Fig. 16. For this purpose we confine the data to those 2150 events which satisfy the selection criteria<sup>41</sup>

$$t < 0.3 \text{ GeV}^2 \quad \text{and} \quad 1.16 < M < 1.30 \text{ GeV}. \quad (13)$$

Figure 21 shows  $d\sigma/dm$ , the distribution of  $p\pi^-$  effective mass for these 2150 events.  $d\sigma/dM$  (the distribution of  $p\pi^+$  effective mass) is displayed in Fig. 22 for the three indicated ranges of  $m$ : 1.60–2.0, 1.30–1.60, and 1.08–1.30 GeV. The distributions of  $d\sigma/dt$  and  $d\sigma/dm_{\Delta\pi}$  ( $m_{\Delta\pi}$  is the effective mass of the  $\Delta^{++}\pi^-$  system) are shown in Fig. 23 for the aforementioned

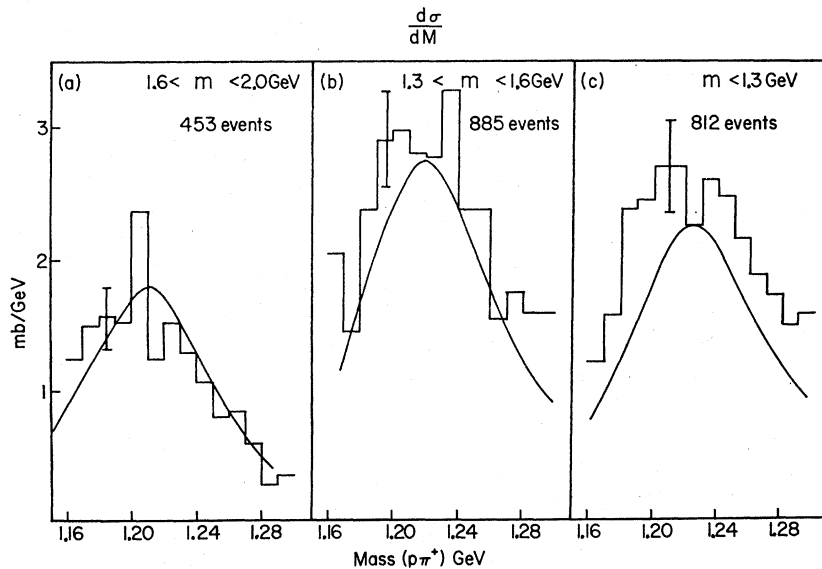


FIG. 22. Differential cross section for  $p\pi^+$  effective mass ( $M$ ) for the  $t$  and  $\Delta^{++}$  selections quoted in Eqs. (13). The distributions (a)–(c) are plotted with the additional indicated restrictions on the  $p\pi^-$  effective mass. The solid curves are the result of the maximum-likelihood fit described in Sec. VIII B.

<sup>41</sup> If both  $M$  combinations fall in the  $\Delta^{++}$  band and both have  $t < 0.3 \text{ GeV}^2$  (this occurs for 160 of the 2150 events), we use the combination with the smallest  $t$ . In either case a given  $M$  combination is associated with the initial state proton which travels in the same c.m. hemisphere. This procedure tends to distort the  $m$  distribution slightly by depleting combinations at intermediate and high  $p\pi^-$  masses and correspondingly adding the other low  $t$  combinations to the low end of the  $m$  spectrum.

<sup>42</sup> See, e.g., E. Ferrari and F. Selleri, *Nuovo Cimento Suppl.* 24, 453 (1962).

<sup>43</sup> See, e.g., J. D. Bjorken and S. D. Drell, *Relativistic Quantum Mechanics* (McGraw-Hill, New York, 1964), section on Feynman rules.

three ranges of  $m$ . The curves superimposed upon the data in Figs. 21–23 inclusive, are the results of an OPE calculation which is described below.

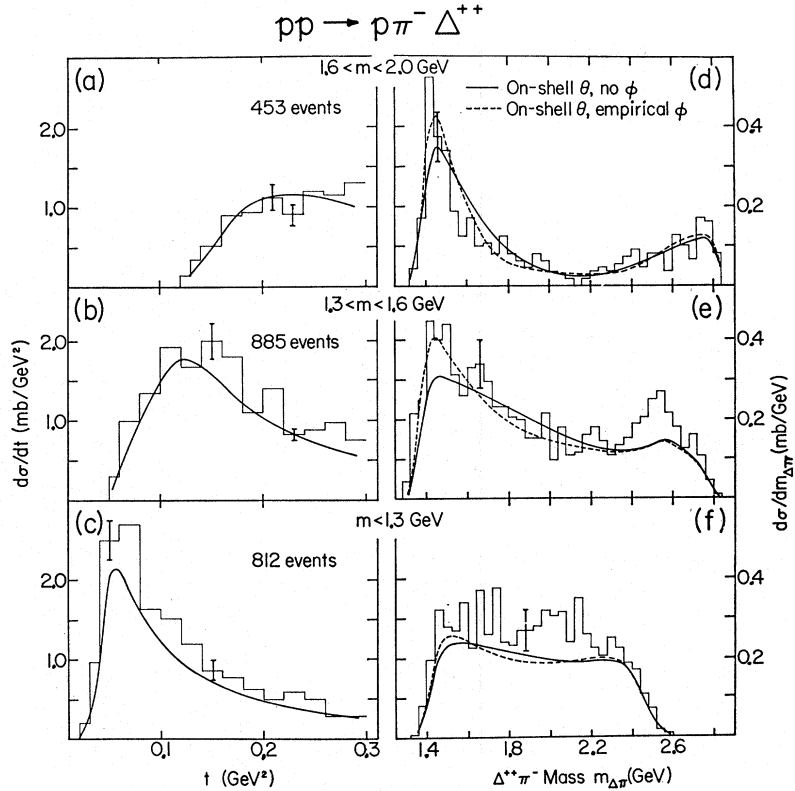
The OPE pole equation for the process of Fig. 17 is given by<sup>42</sup>

$$\frac{d^3\sigma}{dt dM dm} \xrightarrow{t \rightarrow -\mu^2} \frac{2}{4\pi^3 (\hbar c)^2 m_p^2 P_{\text{lab}}^2} \frac{1}{(t + \mu^2)^2} \times [qm^2\sigma(m)][QM^2\sigma(M)]. \quad (14)$$

Here  $q$  and  $Q$  are the magnitudes of the incoming proton momenta in the  $\pi^-p$  and  $\pi^+p$  rest frames, respectively,  $m_p$  and  $\mu$  are the proton and charged pion rest masses, and  $\sigma(m)$  and  $\sigma(M)$  are the on-shell  $\pi^-p$  and  $\pi^+p$  elastic cross sections. The 2 in the numerator of Eq. (14) is due to the two identical nucleons in the initial state.<sup>43</sup> Equation (14) represents a non-interference approximation which we believe to be valid to better than  $\sim 10\%$  at 6.6 GeV/c.  $(\hbar c)^2 = 0.388 \text{ mb GeV}^2$  serves to correct the dimensions in the equation such that all energies and momenta are expressed in units of GeV and all cross sections in units of mb.

Equation (14) is valid only at the pion-exchange pole ( $t = -\mu^2$ ) which is located in the unphysical region of  $t$ . In the past, experimenters have modified Eq. (14) for use in the physical region of the Chew-Low plane by different methods, of which all are basically form-

FIG. 23. (a)–(c) Differential cross section for momentum transfer ( $t$ ) to the  $\Delta^{++}$  for the  $t$  and  $\Delta^{++}$  selections quoted in Eqs. (13). The distributions (a)–(c) are plotted with the additional indicated selections on the  $p\pi^-$  effective mass. (d)–(f) differential cross section for the  $\Delta^{++}\pi^-$  effective mass ( $m_{\Delta\pi}$ ) for the same selections on  $m$  as in (a)–(c). The solid curves on (a)–(c) show the results of the maximum-likelihood fit described in Sec. VIII B. The solid and dashed curves displayed in (d)–(f) are calculated with the different  $dN/d\Omega$  assumptions shown (see Sec. VIII D).



factor approaches. Recently Wolf<sup>44</sup> has been successful in fitting the  $d\sigma/dt$  distributions in both shape and normalization for the quasi-two-body reactions  $\pi^+p \rightarrow \rho^0\Delta^{++}$ ,  $\bar{p}p \rightarrow \bar{\Delta}^-\Delta^{++}$ ,  $p\bar{p} \rightarrow \Delta^{++}n$ , and  $\pi^-p \rightarrow \rho^0n$  over a large range of beam momenta. Wolf modified the pole equation in each case by the vertex form factors suggested by Dürr and Pilkuhn<sup>45</sup> (henceforth referred to as DP-OPE). The DP vertex factors are generalizations of angular momentum barrier factors and modify the individual partial waves at each scattering vertex. Although Wolf dealt only with situations in which one (resonant) partial wave dominates at each vertex, in principle the DP method can be used for situations where several partial waves are present at one (or both) vertices. This is the approach taken in the work reported here. The smooth curves drawn in Figs. 21–23 are the predictions of DP-OPE for  $p\bar{p} \rightarrow \Delta^{++}(p\pi^-)$  calculated as described in the following paragraphs.

The partial-wave structure of the on-mass-shell  $\pi^-p$  cross section is given by

$$\sigma(m) = 4\pi\lambda^2 \sum_{L,J} (J + \frac{1}{2}) |A_{LJ}^{\pi^-p}|^2, \quad (15a)$$

where the  $A_{LJ}^{\pi^-p}$  are given by

$$A_{LJ}^{\pi^-p} = \frac{2}{3}A_{LJ}^{T=\frac{1}{2}} + \frac{1}{3}A_{LJ}^{T=\frac{3}{2}}. \quad (15b)$$

The  $A_{LJ}^T$  are the standard  $\pi N$  partial-wave amplitudes for isotopic-spin  $T$ , orbital and total angular momentum,  $L$  and  $J$ , respectively. The behavior of the  $(J + \frac{1}{2}) |A_{LJ}^{\pi^-p}|^2$  for the first six partial waves<sup>35</sup> for  $m < 1.6$  GeV are shown in Fig. 24. Figure 24 indicates that  $\pi^-p$  elastic scattering can be approximately described by the first four partial waves ( $s_{1/2}$ ,  $p_{1/2}$ ,  $p_{3/2}$ , and  $d_{3/2}$ ) for  $m < 1.6$  GeV. The  $\pi^+p$  elastic cross section in the  $\Delta^{++}(1238)$  region is dominated by the  $p_{3/2}$

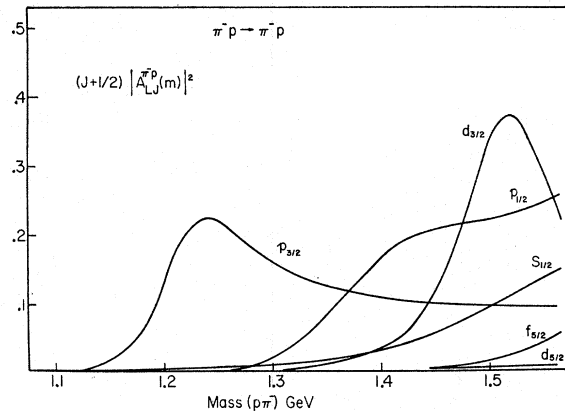


FIG. 24. Behavior of the quantities  $[(J + \frac{1}{2}) |A_{LJ}^{\pi^-p}|^2]$  for  $\pi^-p$  elastic scattering for the first six partial waves for  $m < 1.6$  GeV. The curves were drawn through points derived from the phase-shift analysis of Roper *et al.* (Ref. 35).

<sup>44</sup> G. Wolf, Phys. Rev. Letters 19, 925 (1967); see also Ref. 52.

<sup>45</sup> H. P. Dürr and H. Pilkuhn, Nuovo Cimento 40, 889 (1965).

partial wave, so we take

$$\sigma(M) \approx 8\pi\lambda^2 |A_{p_{3/2} T=\frac{3}{2}}|^2. \quad (16)$$

The DP prescription for continuing the pole equation (14) into the physical region of  $t$  consists of modifying each partial wave separately. We assume that the modification of each partial wave depends only on its  $L$  and  $J$  values and not on its isospin components. The form of the DP modification for the first four partial waves in  $\pi N$  scattering are given by

$$[q\sigma_{s_{1/2}}]_{\text{off shell}} = W[q\sigma_{s_{1/2}}]_{\text{on shell}}, \quad (17a)$$

$$[q\sigma_{p_{1/2}}]_{\text{off shell}} = W^{-1} \left( \frac{q_t}{q} \right)^2 \left( \frac{1+R_{p_{1/2}}^2 q^2}{1+R_{p_{1/2}}^2 q_t^2} \right) [q\sigma_{p_{1/2}}]_{\text{on shell}}, \quad (17b)$$

$$[q\sigma_{p_{3/2}}]_{\text{off shell}} = W \left( \frac{q_t}{q} \right)^2 \left( \frac{1+R_{p_{3/2}}^2 q^2}{1+R_{p_{3/2}}^2 q_t^2} \right) [q\sigma_{p_{3/2}}]_{\text{on shell}}, \quad (17c)$$

$$[q\sigma_{d_{3/2}}]_{\text{off shell}} = W^{-1} \left( \frac{q_t}{q} \right)^4 \left( \frac{9+3R_{d_{3/2}}^2 q^2 + R_{d_{3/2}}^4 q^4}{9+3R_{d_{3/2}}^2 q_t^2 + R_{d_{3/2}}^4 q_t^4} \right) \times [q\sigma_{d_{3/2}}]_{\text{on shell}}, \quad (17d)$$

where

$$W = \frac{(m+m_p)^2 + t}{(m+m_p)^2 - \mu^2}. \quad (17e)$$

The momentum factors  $q_t$  and  $q$  are defined as in Eqs. (8) and (9), respectively. The factors in Eqs. (17) are arrived at by DP in a relativistic generalization of potential-theory results. The  $R_{LJ}$  quantities are free parameters which correspond to radii of interaction in nonrelativistic potential theory. The quantity  $W$  defined by Eq. (17e) is due to the spin- $\frac{1}{2}$  nature of the incoming protons. The multiplicative factors present in the right-hand sides of Eqs. (17) decrease in importance with increasing  $\pi N$  mass and  $R_{LJ}$ , and decreasing  $t$ , and reduce to unity at the pole ( $t = -\mu^2$ ). Thus, for small values of  $t$  and large  $m$  and  $R$  values,  $[q\sigma]_{\text{off shell}}$  can be well approximated by  $[q\sigma]_{\text{on shell}}$ .

Following Wolf, we allow for an additional (moderate) form factor multiplying Eq. (14) of the type  $G(t)^2 = [(c-\mu^2)/(c+t)]^2$ .<sup>46</sup> Wolf quotes  $c = 2.29 \pm 0.27$

<sup>46</sup> This type of form factor was first used by G. Goldhaber *et al.*, Phys. Letters 6, 62 (1963), who fit  $K^+p \rightarrow K^*\Delta$  with no additional vertex factors and found  $c = 0.165$  GeV<sup>2</sup>. It should be recognized that while it is possible to fit individual reactions using just this form factor (provided different values for  $c$  are chosen for each case to give agreement with the data), it is not possible to form a self-consistent phenomenological description of all reactions of the classes  $Xp \rightarrow X\pi^+n$  and  $Xp \rightarrow X\pi^-\Delta^{++}$  unless additional parameters are introduced. DP-OPE does just this in a very economical way (see Ref. 52). Also note that G. Wolf [Phys. Rev. 182, 1538 (1969)] has shown that an improved version of the Dürre-Pilkahn parametrization by Benecke and Dürre provides a

GeV<sup>2</sup> from his fit. Thus  $G(t)$  is only weakly dependent upon  $t$ , a fact which is due to the DP vertex factors tending to a constant at large  $t$  instead of continuing to increase as those in the Born amplitude.

We noted above that  $[q\sigma]_{\text{off shell}} \approx [q\sigma]_{\text{on shell}}$  at small  $t$  and large  $m$ . The dashed curve in Fig. 21 is  $d\sigma/dm$ , obtained after integrating the DP-corrected Eq. (14) over the  $t$  and  $M$  ranges of selection (13). For  $c$  and  $R_{p_{3/2}}$  (or  $R_\Delta$ ) we used Wolf's values (2.3 GeV<sup>2</sup> and 4.0 GeV<sup>-1</sup>, respectively). At the  $\pi^-p$  vertex,  $[q\sigma(m)]_{\text{on shell}}$  was used directly with no off-shell vertex correction [ $\sigma(m)$  was taken from the summary of Focacci and Giacomelli<sup>47</sup>]. The  $p\pi^+$  on-shell cross section was constructed from the phase-shift data of Roper *et al.*<sup>35</sup> Although for  $m \lesssim 1.6$  GeV, the off-shell corrections to the  $\pi^-p$  vertex are necessary as expected, for  $m > 1.6$  GeV the agreement in absolute normalization as well as in the shape of the  $t$ ,  $m$ , and  $M$  dependences in Figs. 21–23 is quite good. We believe this result to be of great interest in connection with the entire Deck problem and the question of diffraction production of  $N^*(1450)$  in the  $\Delta^{++}\pi^-p$  reaction. We defer discussion of this matter to Secs. VIII D, VIII E, and IX.

For the remainder of this section we discuss a maximum-likelihood fit of the off-shell corrected Eq. (14) to the three-dimensional Chew-Low distribution of  $p\bar{p} \rightarrow \Delta^{++}p\pi^-$  for  $m < 1.6$  GeV [in addition to the selections given in Eqs. (13)]. In this fit, the on-shell  $\pi^\pm p$  cross sections were used as input (only the first four partial waves are necessary in this  $m$  region—see Fig. 24) and the likelihood function  $L_i = d^3\sigma/dtdm dM$  was evaluated for each event in the sample. Allowing the parameters  $R_{p_{1/2}}$ ,  $R_{p_{3/2}}$ ,  $R_{d_{3/2}}$ ,  $c$ , and  $R_\Delta$  (at the  $\Delta^{++}$  vertex) to vary, the grand likelihood function

$$\mathcal{L} = \prod_{i=1}^{N \text{ events}} \left( L_i / \int L dt dm dM \right)$$

was maximized<sup>48</sup> using a search technique and the program MINFUN.<sup>49</sup>

Note that since the experimental cross section nowhere appears in the fitting procedure, the fit is just to the shape of the experimental Chew-Low distribution. On the other hand, once the above  $R$  and  $c$  parameters are determined from the fit to the shape of the distribution, they may be used with Eqs. (14) and (17) to calculate absolute predictions of  $d^3\sigma/dtdm dM$ , the projections of which may be compared with the experimental distributions. A good fit implies a successful *inverse pole extrapolation*. That is, in the case

description of Chew-Low distributions out to larger values of  $t$  than the 0.3 GeV<sup>2</sup> used for our DP work and in addition does not need the  $G(t)^2$  form factor. For  $t < 0.3$  GeV<sup>2</sup>, Wolf points out that these two parametrizations are equivalent.

<sup>47</sup> M. N. Focacci and G. Giacomelli, CERN Report No. 66-18, 1966 (unpublished).

<sup>48</sup> See, e.g., Jay Orear, LRL Report No. UCRL 8417, 1958 (unpublished).

<sup>49</sup> W. E. Humphrey, Alvarez Group Programmers Note P-6, 1962 (unpublished).



at hand, we know the on-shell vertex cross sections; a fit is made to the  $t$  and mass dependence of the Chew-Low distribution and we see if we obtain the correct absolute description of the experimental data. Independent of the relevance of DP-OPE to any other pion-exchange reactions, as a functional form for pole extrapolation it is certainly an economical one since only five free parameters are used to extrapolate over a mass region 500 MeV wide.

The best values for the parameters resulting from the maximum-likelihood fit are

$$\begin{aligned} c &= 1.2 \pm 0.5 \text{ GeV}^2, \\ R_\Delta &= 3.5 \pm 0.7 \text{ GeV}^{-1}, \\ R_{p_{1/2}} &= 0.3 \pm 0.9 \text{ GeV}^{-1}, \\ R_{p_{3/2}} &= 2.3 \pm 0.3 \text{ GeV}^{-1}, \\ R_{d_{3/2}} &> 30 \text{ GeV}^{-1}. \end{aligned}$$

The large value for  $R_{d_{3/2}}$  is a reflection of the fact that the off-shell corrections in (17d) are not necessary in the  $m$  range at which the  $d_{3/2}$  partial wave becomes important ( $\sim 1.5$  GeV—see Fig. 24). The solid curves drawn in Figs. 21, 22, and 23(a)–(c) are the  $m$ ,  $M$ , and  $t$  projections calculated with the DP-corrected Eq. (14) using the above values of the five parameters. For  $m > 1.6$  GeV,  $q\sigma(m)$  is given by the on-shell  $\pi^-p$  cross sections, although the above values of  $c$  and  $R_\Delta$  are used in calculating the curves.<sup>50</sup> The agreement of the solid curves with the data is generally rather good, although for the low- $m$  region the normalization is a bit low.<sup>51</sup> (In both  $M$  and  $t$  projections the relative normalizations between the solid curves and the data reflect the same situation as in Fig. 21.) There is, however, excellent agreement between the shapes in all three  $t$  and  $M$  projections.

We conclude that DP-OPE provides a reasonably good (but not exact) functional connection between the Chew-Low distribution for  $p\bar{p} \rightarrow \Delta^{++}$  and the on-shell  $\pi^\pm p$  cross sections at the pion-exchange pole. For a further discussion of the way in which DP-OPE can be used as a tool in extrapolation of experimental distributions to the pion-exchange pole, but in which DP-OPE need not be assumed to be exact, see the analysis of  $p\bar{p} \rightarrow (p\pi^+)n$  at 6.6 GeV/c by Ma *et al.*<sup>52</sup>

<sup>50</sup> Note that for  $m > 1.6$  GeV the solid and dashed curves in Fig. 21 differ in that the  $(c, R_\Delta)$  parameters used are (1.2, 3.5) and (2.3, 4.0), respectively. The calculated  $d\sigma/dm$  is seen to be insensitive to this variation of the parameters.

<sup>51</sup> Note that we have a  $\pm 5\%$  uncertainty in our cross-section normalization (for  $p\bar{p} \rightarrow p\bar{p}\pi^+\pi^-$ ,  $\sigma = 2.70 \pm 0.16$  mb). In addition the  $m$  spectrum may be slightly distorted because of the selection procedure described in Ref. 41. We also ignore the non- $\Delta(1238)$  contribution at the  $\pi^+p$  vertex in the calculation, although this would affect the entire  $d\sigma/dm$  spectrum.

<sup>52</sup> In addition to Wolf's analysis (Ref. 44), other detailed analyses of the following reactions have been performed which further demonstrate that DP-OPE forms a rather good parametrization of the off-mass-shell corrections to the pole equation:  $\pi^-p \rightarrow \rho^0 n$  [E. Malamud and P. Schlein, in *Proceedings of the Conference on  $\pi\pi$  and  $K\pi$  Interactions* (Argonne National Laboratory, Argonne, Ill., 1969), p. 93];  $p\bar{p} \rightarrow \Delta^{++}n$  [Z. M. Ma, G. A. Smith, R. J.

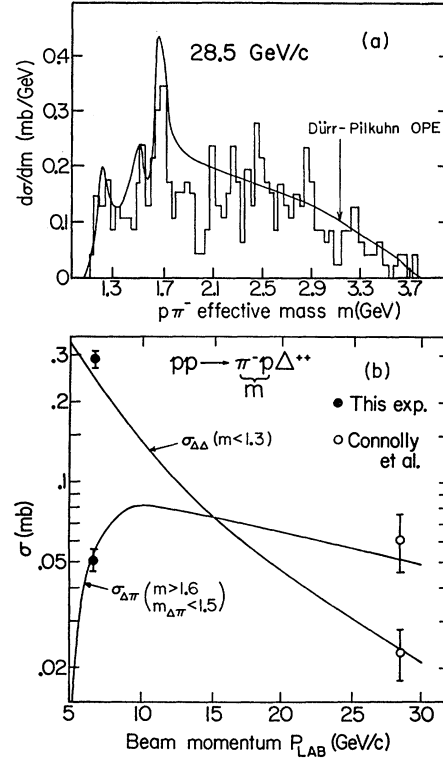


FIG. 25. (a) 28.5-GeV/c differential cross section for  $p\pi^-$  effective mass ( $m$ ), using the  $t$  and  $\Delta^{++}$  selections quoted in Eqs. (13) from Connolly *et al.* (Ref. 21). Except for the difference in beam momentum, the solid curve is equivalent to that in Fig. 21. For  $m > 1.6$  GeV, no off-shell corrections are made at the  $p\pi^-$  vertex. (b) Predicted dependence for  $\sigma_{\Delta\pi}$  ( $m_{\Delta\pi} < 1.5$  GeV) and  $\sigma_{\Delta\Delta}$  ( $m < 1.3$  GeV) (as defined in Sec. VIII C). Our experimental points and those of Connolly *et al.* are shown.

### C. Predictions at Higher Energy

DP-OPE permits us to evaluate the dependence on beam momentum of  $d\sigma/dm$ . Figure 25(a) displays the experimental  $d\sigma/dm$  at 28.5 GeV/c from the BNL experiment of Connolly *et al.*<sup>21</sup> The solid curve is our prediction based on the best-fit parameters obtained in the previous section in fitting the 6.6-GeV/c data. The agreement is seen to be fairly good both in absolute normalization and in shape.

For the  $t$  and  $M$  selections of Eqs. (13) and for  $m > 1.6$  GeV, the predicted dependence on  $P_{\text{lab}}$  of the cross section for  $m_{\Delta\pi} < 1.5$  GeV is shown in Fig. 25(b). As discussed in detail in the following section, in order to calculate the  $\Delta\pi$  mass spectrum from  $d^3\sigma/dtdm dM$ , it is necessary to assume a form of  $dN/d\Omega$ , the angular distribution in the  $\pi^-p$  rest frame. As an approximation

Sprafka, E. Colton, and P. Schlein, Phys. Rev. Letters **23**, 342 (1969)];  $K^+p \rightarrow K^*\Delta^{++}$  [T. Trippe, C. Y. Chien, E. Malamud, J. Mellema, P. Schlein, W. Slater, D. Stork, and H. Ticho, Phys. Letters **28B**, 203 (1968)]. These analyses, as well as a discussion of  $K^-p \rightarrow K^*n$ , are summarized in the review talk of Peter E. Schlein, in *Meson Spectroscopy*, edited by C. Baltay and A. H. Rosenfeld (Benjamin, New York, 1968), p. 161.

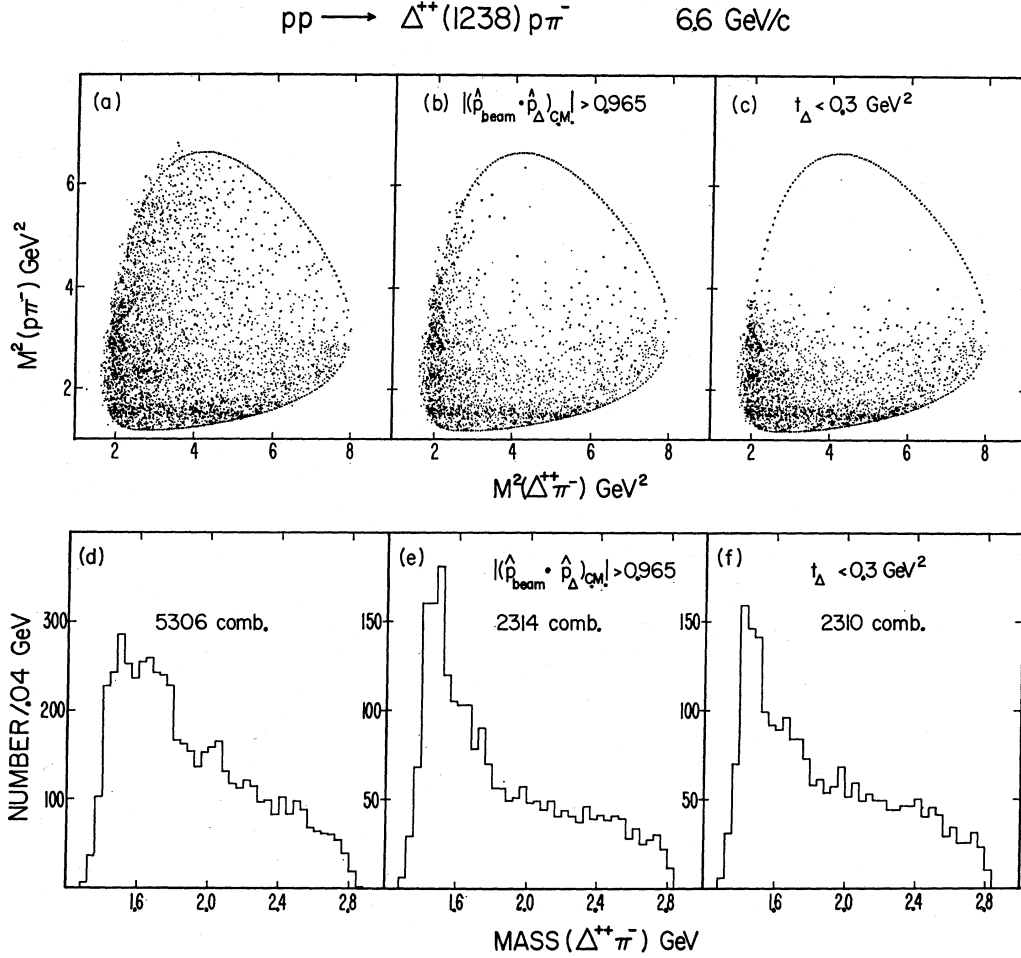


FIG. 26. Dalitz plots for  $pp \rightarrow \Delta^{++} p\pi^-$  for (a) all combinations; (b) only events with  $\Delta^{++}$  c.m. production angle cosine  $|\cos\theta_{\Delta^{++}}^{c.m.}| > 0.965$ ; (c) only events with momentum transfer to the  $\Delta^{++}$ ,  $t < 0.3 \text{ GeV}^2$ ; (d)–(f) are the corresponding projections of  $\Delta^{++}\pi^-$  effective mass.

to  $dN/d\Omega$  in this calculation, we used our empirical  $dN/d\Omega$  for  $m < 2.3 \text{ GeV}$ ; for  $m > 2.3 \text{ GeV}$ , the  $p\pi^-$  scattering was taken to be a diffractive  $e^{-at}$  form. We used a value of  $a = 7.7 \text{ GeV}^{-2}$  obtained from the data summary of Focacci and Giacomelli.<sup>47</sup> For comparison with  $\sigma_{\Delta\pi}$ , the calculated cross section for double isobar production  $pp \rightarrow \Delta^{++}\Delta^0(1238)$ ,  $\sigma_{\Delta\Delta}$  ( $m < 1.3 \text{ GeV}$ ) is also shown in Fig. 25(b). It is interesting to note the weak dependence of  $\sigma_{\Delta\pi}$  on  $P_{\text{lab}}$  (also observed using diffraction-dissociation models) compared with the approximately  $P_{\text{lab}}^{-2}$  falloff of  $\sigma_{\Delta\Delta}$ . This is due to the fact that in the  $\sigma_{\Delta\pi}$  calculation, an integration is made over the entire range  $m > 1.6 \text{ GeV}$  (the  $P_{\text{lab}}^{-2}$  dependence occurs only for fixed vertex mass selection). The diffraction scattering is implicit in the  $p\pi^-$  vertex, although the calculation is done within an OPE framework. The corresponding experimental points at 6.6 and 28.5 GeV/c<sup>21</sup> are seen to be in reasonable agreement with the respective  $\sigma_{\Delta\pi}$  and  $\sigma_{\Delta\Delta}$  curves.

#### D. $m_{\Delta\pi}$ Distribution

$\Delta^{++}p\pi^-$  Dalitz plots are presented in Figs. 26(a)–26(c) along with the respective  $\Delta^{++}\pi^-$  mass projections in Figs. 26(d)–26(f). Figure 26(a) contains all  $\Delta^{++}\pi^-$  combinations, while in Figs. 26(b) and 26(c) events are plotted with the additional restrictions  $|\cos\theta_{\Delta^{++}}^{c.m.}| > 0.965$  and  $t < 0.3 \text{ GeV}^2$ , respectively. The peripheral  $\Delta^{++}$  component is thereby enhanced in Figs. 26(b) and 26(c), although in both there is a kinematic suppression at large  $\pi^-p$  mass. All three of the Dalitz plots have nonuniform populations. The points tend to cluster along the boundaries of low  $p\pi^-$  and low  $\Delta^{++}\pi^-$  mass. This effect is especially pronounced for the peripheral  $\Delta^{++}p\pi^-$  events. The peripheral mass projections given in Figs. 26(e) and 26(f) exhibit a striking enhancement centered at  $\sim 1.45 \text{ GeV}$ . This enhancement is the same one observed in the shaded portion of Fig. 9(a). The peripheral Dalitz plots indicate further that the low-mass  $\Delta^{++}\pi^-$  enhancement is mainly due

to those events with a pronounced forward scattering in the  $p\pi^-$  rest system.

*Kinematic Relationship between  $m_{\Delta\pi}$ ,  $t_p$ , and  $\pi^-p$  "Scattering" Angle  $\theta$*

We now discuss the kinematic relationship between  $m_{\Delta\pi^2}$ , the "scattering" angle  $\theta$  in the  $\pi^-p$  rest frame, and the proton-to-proton momentum transfer  $t_p$ . For the purpose of illustration, let us assume that for any  $\pi^-p$  mass  $m$ , the momentum transfer of proton to  $\Delta^{++}$ ,  $t$ , has its minimum value; in other words, the c.m. production angle cosine of the  $\Delta^{++}$   $|\cos\theta_{\Delta^{++}}| = 1.0$ . This is approximately the case, for example, for the events in Figs. 26(b) and 26(e). For this particular configuration, the longitudinal "decay" angle of the  $\pi^-p$  system, the cosine of which scales from  $-1.0$  to  $+1.0$  along a line of constant  $\pi^-p$  mass on the Dalitz plots of Fig. 26, is the same angle used to evaluate the  $\pi^-p$  moments in Sec. VIII A. Furthermore, the momentum transfer to the proton  $t_p$  is proportional to the cosine of this angle:

$$m_{\Delta\pi^2} \propto \theta \propto t_p.$$

For a given value of  $\pi^-p$  mass,  $m_{\Delta\pi^2}$  and  $t_p$  have their minimum values when  $\cos\theta = +1$ . It may thus be seen that the observed dependence of the  $t_p$  distribution on the three-body mass, summarized in Figs. 9 and 10, is, qualitatively speaking, a kinematic consequence of the experimental situation displayed in the Dalitz plots of Fig. 26. The low-mass  $\Delta\pi$  system dominantly arises from large  $\pi^-p$  mass which is characterized by  $\cos\theta \sim 1$  dominance and thus minimum  $t_p$ .

*Review of Argument of Gellert et al.*

Gellert *et al.*,<sup>9</sup> in a preliminary analysis of  $\sim \frac{1}{3}$  of our final statistics, argued at the 1966 Rochester Meeting that the fair agreement between the observed  $\pi^-p$  moments and on-shell  $\pi^-p$  scattering implied that the data were dominated by the process of Fig. 17 and thus that the low-mass  $\Delta^{++}\pi^-$  enhancement was dominantly kinematic in nature. In other words, referring to the Dalitz-plot distribution in Fig. 26(b), for example, for a given  $\pi^-p$  mass bin we understood (approximately) the  $m_{\Delta\pi^2}$  distribution. The difficulty with that argument was that since DP-OPE had not yet emerged on the scene and therefore the associated phenomenological summaries of OPE had not yet been done, it was not possible to perform a reliable integration over  $\pi^-p$  mass to calculate the detailed shape and normalization of the  $\Delta^{++}\pi^-$  spectrum due to all  $\pi^-p$  masses of interest.

*Calculation of  $m_{\Delta\pi}$  Distribution Using DP-OPE*

DP-OPE can be used to calculate the reflected  $\Delta^{++}\pi^-$  mass distributions. This amounts to a somewhat more sophisticated Deck calculation, more sophisticated in the sense that the  $t, m, M$  dependence used is that of an internally consistent phenomenological description

of the complete set of reactions of the classes  $Xp \rightarrow X\pi^-\Delta^{++}$  and  $Xp \rightarrow X\pi^+n$ . In Figs. 23(d)–23(f) are displayed the experimental  $\Delta^{++}\pi^-$  mass distributions for the three aforementioned ranges in  $m$ : 1.6–2.0, 1.3–1.6, and 1.08–1.3 GeV, respectively. The enhancements at low  $\Delta^{++}\pi^-$  mass ( $\sim 1450$  MeV) are apparent, the peaking for the large- $m$  selection being especially pronounced. This enhancement is the same as that observed in Figs. 9(a), 26(e), and 26(f).

Given the expression for  $d^3\sigma/dt dM dm$  [DP-modified Eq. (14)], the additional specification of the angular distribution  $dN/d\Omega(\theta, \phi)$  at the  $p\pi^-$  vertex as a function of  $m$  completely determines the  $m_{\Delta\pi}$  distribution (alternatively, the dependence on the Lorentz-invariant variables  $m_{\Delta\pi}$  and  $t_p$  provides a complete description of the data). We should stress the trivial but important point that the assumed  $dN/d\Omega(\theta, \phi)$  distribution only affects the *shape* of any calculated  $d\sigma/dm_{\Delta\pi}$  distribution; the magnitude is already fixed by the  $d^3\sigma/dt dM dm$  DP-OPE distribution. Thus, for example, the areas under the calculated  $d\sigma/dm_{\Delta\pi}$  curves in Figs. 23(d)–23(f) are identical to the areas under the  $d\sigma/dM$  curve in Fig. 21 for the corresponding  $m$  ranges. This means that the spherical harmonic moments  $\langle Y_L^M \rangle$  evaluated in the  $\pi^-p$  rest frame contain exactly equivalent information as the shape of the  $m_{\Delta\pi}$  distribution (assuming that the same  $t, M, m$  selection is made).

If the conventional  $t$ -channel coordinate system is used for the polar angle  $\theta$  and the Treiman-Yang angle  $\phi$  at the  $\pi^-p$  vertex ( $\hat{y} \sim \hat{n}$  and  $\hat{z} = \hat{P}_{\text{incident}}$  as seen in the  $\pi^-p$  rest frame),  $m_{\Delta\pi}$  can be shown to be kinematically related to  $\theta$  and  $\phi$  via the expression

$$m_{\Delta\pi^2} = m_{\Delta^2} + \mu^2 + 2E_{\Delta}E_{\pi} + 2Qq(\cos\theta \cos\theta_{\Delta} - \sin\theta \sin\theta_{\Delta} \cos\phi). \quad (18)$$

All angles, energies, and momenta are evaluated in the  $\pi^-p$  rest frame.  $\theta_{\Delta}$  is the polar angle of the  $\Delta^{++}$ ,  $Q$  and  $q$  are the momenta of the  $\Delta^{++}$  and the  $\pi^-$ , and  $E_{\Delta}$  and  $E_{\pi}$  are the energies of the  $\Delta^{++}$  and  $\pi^-$ .

We show, in Figs. 23(d)–23(f),  $d\sigma/dm_{\Delta\pi}$  distributions calculated for several  $dN/d\Omega(\theta, \phi)$  assumptions. The solid curves are calculated using the on-mass-shell  $\theta$  dependence of  $\pi^-p$  elastic scattering and assume no  $\phi$  dependence (in contradistinction to the data as shown below). The dashed curves are calculated in the same way except that the observed  $M \neq 0$   $\langle \text{Re}Y_L^M \rangle$  moments for  $L \leq 6$  are added to  $dN/d\Omega$ . *Inasmuch as the shape of the experimental  $d\sigma/dm_{\Delta\pi}$  distributions can only be reproduced if exactly the experimental  $dN/d\Omega(\theta, \phi)$  distribution is used in the calculation (because of the above-stated kinematic equivalence between the  $dN/d\Omega$  distribution and the shape of the  $d\sigma/dm_{\Delta\pi}$  distribution—for the same  $t, M, m$  selection), it should come as no surprise that both the solid and dashed curves fail to reproduce the narrow width of the  $\sim 1450$ -MeV  $\Delta\pi$  enhancement in Fig. 23(d).* This difficulty can be traced to the fact that the experimental  $dN/d \cos\theta$  for  $m > 1.6$  GeV is more

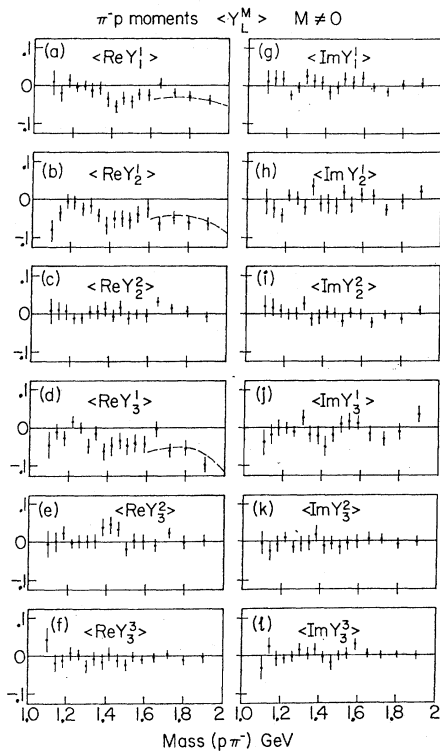


FIG. 27. Nonzero  $M$  moments  $\langle \text{Re} Y_L^M \rangle$  and  $\langle \text{Im} Y_L^M \rangle$  for  $L, M \leq 3$ , of the outgoing proton evaluated in the  $p\pi^-$  rest frame as a function of the  $p\pi^-$  effective mass. The moments are calculated for the 2314  $\Delta^{++}p\pi^-$  combinations with  $|\cos\theta_{\Delta^{++}p\pi^-}| > 0.965$ . The coordinate system uses for its  $z$  axis the direction of the appropriate incoming proton as seen in the  $p\pi^-$  rest frame. The normal to the production plane is used for the  $y$  axis. The dashed curves superimposed on the  $\langle \text{Re} Y_L^1 \rangle$  moments are the predictions of the Reggeized Deck-model calculation described in Sec. VIII E, in which a linear pion trajectory of unit slope is assumed.

forward peaked than in on-mass-shell  $\pi^-p$  scattering. Our empirical  $dN/d\Omega$  distribution has significant moments with larger  $L$  values ( $L_{\text{max}} \geq 10$ ) than appear in on-mass-shell  $\pi^-p$  scattering in our mass region ( $L_{\text{max}} \approx 6$ ). This behavior was manifest in Fig. 19 as a tendency for the  $L \geq 4$  moments to exceed the on-mass-shell curves above 1.7 GeV. We draw attention to the fact that, despite this sharpened  $\theta$  distribution as compared to the on-shell  $\theta$  distribution and the observed  $\phi$  dependence discussed in the next section, DP-OPE does account rather well for the intensity distribution of all events. As for Figs. 23(e) and 23(f), aside from the slightly low normalization for  $m < 1.6$  GeV, the curves do reproduce the data rather well.

#### Treiman-Yang Angular Dependence

This dependence can only be completely displayed if the spherical harmonic moments  $\langle Y_L^M \rangle$  are evaluated. Our experimental moments are illustrated<sup>53</sup> in Figs. 27

<sup>53</sup> We take this opportunity to point out that any histogram of  $\phi$  contains only information on  $\cos M\phi$  for those  $\langle \text{Re} Y_L^M \rangle$  moments which have  $(L+M)$  even. Since we find all the  $\phi$  depen-

and 28 for  $L \leq 6$ . The  $\langle \text{Im} Y_L^M \rangle$  are all consistent with zero, as required by parity conservation.<sup>54</sup> The  $\langle \text{Re} Y_L^1 \rangle$  are significant and of comparable magnitude ( $\sim -0.05$ ) for  $L$  at least up to 6. The dashed curves in Figs. 27(a), 27(b), and 27(d) and the dashed curves in Figs. 28(a)–28(c) are the results of a calculation described in the next section. In connection with our observed Treiman-Yang dependence, it is to be noted that the entire contribution seems to be associated with  $\cos M\phi$  terms with  $M = 1$ .

#### E. Models with Explicit Dependence on $m_{\Delta\pi}$

We have seen above that DP-OPE is successful in accounting in shape and magnitude for the experimental distribution in  $m$ ,  $M$ , and  $t$  (see Figs. 21–23 and Sec. VIII B). The second essential observation is that the  $(\theta, \phi)$  angular distribution  $dN/d\Omega$  at the  $\pi^-p$  vertex differs from on-shell  $\pi^-p$  scattering in two main ways: The first is that, while the observed  $\theta$  distribution has gross features very similar to the on-shell  $\theta$  distribution, it is more sharply forward peaked for  $m \gtrsim 1.6$  GeV; the

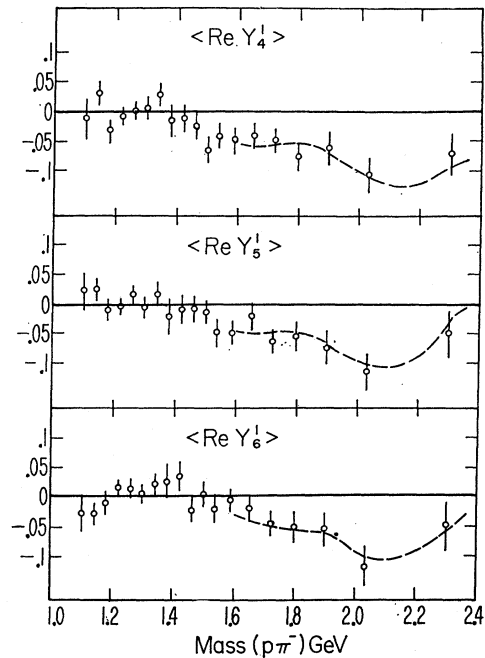


FIG. 28.  $\langle \text{Re} Y_L^1 \rangle$  moments in the  $\pi^-p$  rest frame for  $L=4, 5$ , and 6. The moments were evaluated in the same way as those in Fig. 27. The dashed curves here are calculated by the same method as the dashed curves in Fig. 27.

dence arising from the  $M=1$  moments, a  $\phi$  projection (in our case) contains only information for the  $L=1, 3, 5$  moments. A flat Treiman-Yang projection does not require all  $\phi$  dependence to be absent; for example,  $\langle \text{Re} Y_2^1 \rangle$  or  $\langle \text{Re} Y_3^2 \rangle$ , etc., could still be nonzero.

<sup>54</sup> Note that this is only true if the  $y$  axis is taken to be the normal to the production plane. The parity-conservation requirement of up-down symmetry of single-particle distributions around the production plane is then translated to predict that all  $\sin m\phi$  terms vanish.

second is the presence of a significant dependence on Treiman-Yang angle  $\phi$ , dominantly due to  $\langle \text{Re}Y_L^1 \rangle$  moments.

Because of the aforementioned kinematic relationship between  $dN/d\Omega(\theta, \phi)$  and  $d\sigma/dm_{\Delta\pi}$ , it is thus not possible with a Deck calculation which uses an on-shell  $dN/d\Omega$  distribution to correctly obtain the shape of  $d\sigma/dm_{\Delta\pi}$ . There are two possible equivalent solutions: either (a) perform the Deck calculation using a  $dN/d\Omega$  distribution which differs from the on-shell distribution, or (b) introduce an explicit dependence on  $m_{\Delta\pi}$  into the calculation.

The first of these possibilities, i.e., modifying the  $dN/d\Omega$  distribution, might possibly be accomplished by an absorption model. On the other hand, although the absorption model as currently formulated<sup>55</sup> introduces  $\phi$  dependences such as seen in Figs. 27 and 28, it does not introduce higher  $L$  values in the  $\pi^-p$  angular distribution than those already present in the on-shell scattering. There seems to be some evidence for the presence of such moments. Thus it does not seem that the current absorption model can account for the shape of the  $\Delta^{++}\pi^-$  (1450) enhancement. In any case, to the best of our knowledge, there does not yet exist in the literature an appropriate absorption-model calculation for  $p\bar{p} \rightarrow \Delta^{++}p\pi^-$  for the  $m > 1.6$ -GeV region. We turn, therefore, to the class of models which contains an explicit dependence on  $m_{\Delta\pi}$ .

The explicit dependence on  $m_{\Delta\pi}$  can be obtained in either of two perhaps approximately equivalent ways: one can (a) Reggeize the exchange  $\pi$  or (b) introduce a final-state  $\Delta^{++}\pi^-$  interaction.

It has been shown by Berger<sup>56</sup> that if the exchanged  $\pi$  in the reaction  $\pi p \rightarrow \pi p p$  is Reggeized, a dependence on  $m_{p\pi}$  is introduced into the matrix element which has the desired effect of sharpening the low-mass  $\rho\pi$  ( $A_1$ ) enhancement. An application of this Reggeized Deck model to  $p\bar{p} \rightarrow p\bar{p}\pi^-\Delta^{++}$  at 6.6 GeV/c<sup>10</sup> permits the  $\Delta^{++}\pi^-$  (1450) enhancement to be fit fairly well for  $m > 1.34$  GeV. Subsequent investigations of  $p\bar{p} \rightarrow p\bar{p}\pi^-\Delta^{++}$  at 7.9 GeV/c,<sup>57</sup> 16 GeV/c,<sup>58</sup> and 28.5 GeV/c<sup>59</sup> yield similar results. In the remainder of this section, we review the application of this Reggeized exchange model<sup>60</sup> to the peripheral  $\Delta^{++}p\pi^-$  sample considered in the previous section ( $m > 1.6$  GeV).

Before continuing, it is important to point out that

<sup>55</sup> See, e.g., J. D. Jackson, invited paper to the Conference on High-Energy Two-Body Reactions held at the State University of New York, Stony Brook, New York, 1966 (unpublished).

<sup>56</sup> Edmond L. Berger, Phys. Rev. **166**, 1525 (1968).

<sup>57</sup> D. F. Grether and R. D. Sard, Nucl. Phys. **B14**, 381 (1969).

<sup>58</sup> J. G. Rushbrooke and J. R. Williams, Phys. Rev. Letters **22**, 248 (1969).

<sup>59</sup> Edmond L. Berger, Phys. Rev. **179**, 1567 (1969).

<sup>60</sup> For background, see K. A. Ter-Martirosyan, Nucl. Phys. **68**, 591 (1964); T. W. B. Kibble, Phys. Rev. **131**, 2282 (1963); F. Zachariassen and G. Zweig, *ibid.* **166**, 1326 (1967); H. M. Chan, K. Kajantie, and G. Ranit, Nuovo Cimento **49A**, 1159 (1967); **51A**, 696 (1967); N. F. Bali, G. Chew, and A. Pignotti, Phys. Rev. Letters **19**, 614 (1967); Phys. Rev. **163**, 1572 (1967).

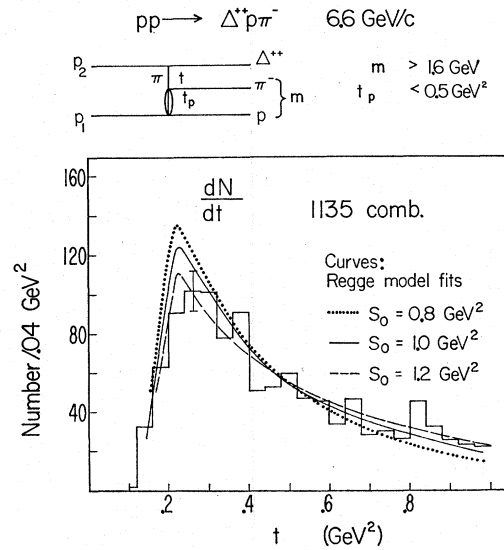


FIG. 29. Distribution of  $t$  for the 1135  $\Delta^{++}p\pi^-$  combinations with  $l < 1.0$  GeV<sup>2</sup>,  $t_p < 0.5$  GeV<sup>2</sup>, and  $m > 1.6$  GeV. The curves drawn are the results of integrating Eq. (21) with  $\lambda = 6$  GeV<sup>-2</sup> and  $\alpha' = 1.4$  GeV<sup>-2</sup>. Dotted curve,  $S_0 = 0.8$  GeV<sup>2</sup>; solid curve,  $S_0 = 1.0$  GeV<sup>2</sup>; and dashed curve  $S_0 = 1.2$  GeV<sup>2</sup>. The curves are normalized to the data although, as discussed in the text and shown in Table III, the calculated and experimental cross sections are in agreement. The inset at the top describes the multiperipheral process which is considered in the calculation.

in these calculations a linear pion trajectory is assumed:

$$\alpha_\pi = -\alpha'(t + \mu^2), \quad (19)$$

in which the slope  $\alpha'$  is of order unity and the minus sign arises because of our choice of metric; there is, however, no experimental evidence in quasi-two-body processes that this is the slope of the pion trajectory. On the contrary, all existing evidence is that the slope is rather flat, perhaps zero. A trajectory of the form (19) would predict, for example, that the  $t$  distributions of processes like  $\pi^+p \rightarrow \rho^0\Delta^{++}$ ,  $\pi^-p \rightarrow \rho^0n$ ,  $K^+p \rightarrow K^*\Delta^{++}$ , etc., would have increasingly larger slopes as one goes to higher beam momentum. This behavior is antithetical to that embodied in the pole equation (14) (even when modified by the DP factors) which has as the only dependence on  $P_{\text{lab}}$  the multiplicative  $P_{\text{lab}}^{-2}$  scale factor. Since there have been various impressive demonstrations that DP-OPE fits experimental  $t$  distributions both in and out of vertex resonance regions,<sup>44,46,52</sup> there is no experimental reason to assume that  $\alpha' \neq 0$ . Wolf,<sup>46</sup> for example, quotes a value of the slope of a linear pion trajectory of  $\alpha' = -(0.051 \pm 0.062)$  GeV<sup>-2</sup>. Studies of the pion-exchange-dominated photo-production process  $\gamma p \rightarrow \pi^+n$  lead to a similar conclusion.<sup>61</sup>

Because of this situation, we regard the Reggeized Deck model described here purely as a phenomenological description of the data with an added degree of

<sup>61</sup> A. M. Boyarski *et al.*, Phys. Rev. Letters **20**, 300 (1968).

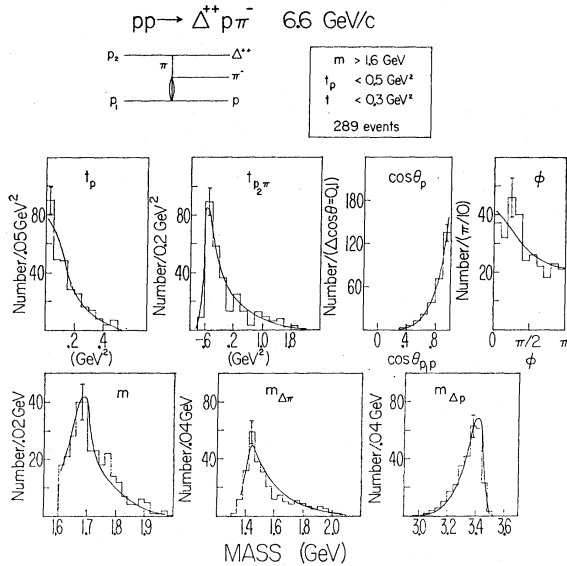


FIG. 30. Distributions for the 289 events satisfying the restrictions of Eqs. (20). (a)  $t_p$ , (b)  $t$ , (c)  $\cos\theta_p$ , (d)  $\phi$ , (e)  $m$ , (f)  $m_{\Delta\pi}$ , and (g)  $m_{\Delta p}$ . The smooth curves drawn through the data are the predictions of Eq. (21) using  $\lambda=6 \text{ GeV}^{-2}$ ,  $S_0=1.0 \text{ GeV}^2$ , and  $\alpha' = 1.4 \text{ GeV}^{-2}$  for the multiperipheral process depicted at the top. In each case, for purposes of the figure, the curve is normalized to the data although, as discussed in the text, the absolute normalization of the calculation is in good agreement with the experimental cross section.

freedom over DP-OPE (the explicit  $m_{\Delta\pi}$  dependence). This model has its source in the multi-Regge-exchange model<sup>60</sup> which can be used to describe our process shown as the inset in Fig. 29 for large  $m_{\Delta\pi}$  and large  $m$ . Berger has suggested that this model be extended down to the low- $m_{\Delta\pi}$  "Deck" region. This extension of the model might find its validity (at least in some average sense) in the duality arguments of Dolen, Horn, and Schmid<sup>62</sup> as discussed by Chew and Pignotti<sup>63</sup> and others. We defer to Sec. IX a more detailed discussion of the significance of this model (to be now described) in connection with what we have referred to above as our "un-Reggeized" Deck calculation and our suggested final-state  $\pi\Delta$  interaction model.

#### Berger Reggeized Deck Model

In order to enhance the contribution of the multiperipheral process shown as the inset in Fig. 29, we impose the restriction

$$t_p < 0.5 \text{ GeV}^2 \quad (20a)$$

in addition to the selections

$$1.16 < M < 1.30 \text{ GeV}, \quad (20b)$$

$$m > 1.6 \text{ GeV}, \quad (20c)$$

<sup>62</sup> R. Dolen, D. Horn, and C. Schmid, Phys. Rev. 166, 1768 (1968).

<sup>63</sup> G. F. Chew and A. Pignotti, Phys. Rev. Letters 20, 1078 (1968).

$$t < 0.3 \text{ GeV}^2. \quad (20d)$$

289 events remain after these cuts. This corresponds to an experimental cross section of  $104 \mu\text{b}$ . The experimental distribution in  $t$  is given in Fig. 29 out to  $t=1.0 \text{ GeV}^2$ . The remaining experimental distributions are given in Fig. 30, where a more elaborate but self-evident notation is used to describe the large number of redundant but interesting variables. The curves in Figs. 29 and 30 are the predictions of the Reggeized Deck calculation described in the following paragraphs.

The conventional procedure followed in the Reggeized Deck calculations is to determine the over-all normalization by requiring  $(d\sigma/dt)_{\text{Regge}}$  to reduce to the pion-exchange pole equation in the vicinity of the pole. Since the final normalization will be determined in this way, we do not bother to write out the multiplicative constants in the following equations.

The  $\Delta^{++}$  in  $pp \rightarrow p\pi^-\Delta^{++}$  is approximated as a particle of definite mass, thus reducing the problem to consideration of a three-body final state. The differential cross section is given by<sup>64</sup>

$$\frac{d^4\sigma}{dt d\Omega dm d\Omega} \propto \frac{q}{m_p^2 P_{\text{lab}}^2} (\sum |A|^2), \quad (21)$$

where  $d\Omega$  describes the angles in the  $p\pi^-$  rest frame and the matrix element is given by the Regge form approximated by<sup>56,59</sup>

$$\sum |A|^2 \propto \frac{(\pi\alpha')^2}{1 - \cos\pi\alpha_\pi} (\sum |A_{\pi^- p}|^2) \left(\frac{R}{S_0}\right)^{2\alpha_\pi}, \quad (22a)$$

$$R = m_{\Delta\pi}^2 + t_p - m_p^2 - (m_{\Delta}^2 - m_p^2 + t)(\mu^2 + t_p + t)/2t. \quad (22b)$$

$t$  is positive in the physical region,  $S_0$  is an adjustable parameter in the phenomenology (of order unity), and  $A_{\pi^- p}$  is the amplitude for the elastic scattering of a Reggeized pion on a proton.

With the assumption that  $\alpha_\pi$  is a linear function of  $t$  [Eq. (19)], the first factor in Eq. (22a) reduces at small  $t$  to the pion propagator  $(t+\mu^2)^{-2}$ . Since this approximation is valid to better than the 90% level for the  $t$  region considered, there is no essential difference in the Reggeized and un-Reggeized cases arising from this factor. As stated above,  $\alpha'$  is usually assumed to be of order unity. The third factor in Eq. (22a) contains the explicit dependence on  $m_{\Delta\pi}$  which Berger<sup>56</sup> emphasized has the effect of sharpening the low-mass Deck enhancement. The kinematically related predictions of the angular distribution in the  $\pi^-p$  c.m. system are also thereby brought into agreement with the data.<sup>10</sup>

The  $\pi^-p$  vertex matrix element factor in Eq. (22a) is related to the physical  $\pi^-p$  elastic-scattering differential cross section via the usual expression for two-

<sup>64</sup> See, e.g., M. Jacob, in *Strong Interaction Physics* (Benjamin, New York, 1964), pp. 10-11; also R. Hagedorn, *Relativistic Kinematics* (Benjamin, New York, 1963), Secs. 7-4 and 7-5.

body scattering<sup>64</sup>:

$$\frac{d\sigma}{d\Omega} \propto \frac{1}{m^2} (\sum |A_{\pi^-p}|^2). \quad (23a)$$

Another method uses the optical theorem and assumes the  $\pi^-p$  amplitude to be purely imaginary in the forward direction:

$$q^2 \sigma^2 e^{-\lambda t_p} \propto \frac{1}{m^2} (\sum |A_{\pi^-p}|^2), \quad (23b)$$

where  $q$  is the momentum in the  $\pi^-p$  rest frame.

Equation (21) was integrated numerically for various values of  $S_0$ ,  $\alpha'$ , and  $\lambda$  and the results were compared with the experimental distributions shown in Figs. 29 and 30. The curves (shown in Figs. 29 and 30) are calculated using Eqs. (21), (22), and (23b), with  $S_0=1$  GeV<sup>2</sup>,  $\alpha'=1.4$  GeV<sup>-2</sup>, and  $\lambda=6$  GeV<sup>-2</sup>; although, as discussed in the next section, the absolute normalization agreement is quite good, the curves shown in Figs. 29 and 30 are simply normalized to the 289-event sample. The value of  $\lambda$  used may be compared with the slope for diffractive on-shell  $\pi^-p$  scattering in our  $m$  range of  $\sim 7.5$  GeV<sup>-2</sup>.<sup>47</sup>

#### Absolute Normalization

To determine the absolute normalization of the calculation, we normalize to the pole equation as  $t \rightarrow -\mu^2$ . In this limit  $\alpha_\pi \rightarrow 0$ . Combining Eqs. (21), (22), and (23a), we have in this limit

$$\frac{d^4\sigma}{dt dm d\Omega} \propto \frac{1}{m_p^2 P_{\text{lab}}^2} \frac{1}{(t+\mu^2)^2} q m^2 \frac{d\sigma}{d\Omega} \quad (24a)$$

or

$$\frac{d^2\sigma}{dt dm} \propto \frac{1}{m_p^2 P_{\text{lab}}^2} \frac{1}{(t+\mu^2)^2} q m^2 \sigma(m). \quad (24b)$$

Equations (24) are to be compared with the pole equation [Eq. (14)] integrated over the  $p\pi^+$  mass selection used in our sample [Eq. (20b)] (this procedure gives a somewhat smaller contribution than integration of the tails of a Breit-Wigner distribution):

$$\frac{d^2\sigma}{dt dm} = \frac{2}{4\pi^3 (\hbar c)^2 m_p^2 P_{\text{lab}}^2} \frac{1}{(t+\mu^2)^2} q m^2 \sigma(m) \times \int_{1.16}^{1.30} Q M^2 \sigma(M) dM. \quad (25)$$

Using the known<sup>47</sup> elastic  $\pi^+p$  cross section (this adds an  $\sim 10\%$  contribution in addition to the  $p_{3/2} \Delta^{++}$  cross section) in the integral on the right-hand side, the value of the integral is found to be

$$\int_{1.16}^{1.30} Q M^2 \sigma(M) dM = 6.60 \text{ mb GeV}^4. \quad (26)$$

TABLE III. Dependence of calculated cross section [from Eq. (21)] upon  $\alpha'$  and  $\lambda$ ;  $S_0=1$  GeV<sup>2</sup>. Cross sections in  $\mu\text{b}$  ( $\sigma_{\text{expt}}=104 \mu\text{b}$ ).

$\lambda$ (GeV <sup>-2</sup> )	$\alpha'$ (GeV <sup>-2</sup> )	1.0	1.2	1.4
5		119	122	126
6		104	106	110
7		91	94	97
8		81	84	87
9		73	75	78

Equating the right-hand side of Eqs. (25) and (24b), we find that the over-all normalization constant in Eqs. (24) is 0.106 mb GeV<sup>4</sup>.

Table III shows the predicted integrated cross section corresponding to the selection criteria of Eqs. (20) for several different values of  $\lambda$  and  $\alpha'$ .  $S_0$  is equal to 1 GeV<sup>2</sup> for the entire table. The corresponding experimental cross section is 104  $\mu\text{b}$ . This number agrees well with the value of 110  $\mu\text{b}$  obtained when  $\lambda=6$  GeV<sup>-2</sup> and  $\alpha'=1.4$  GeV<sup>-2</sup> (used for the curve calculations in Figs. 29 and 30).

#### $\pi^-p$ Angular Distribution

In order to study in further detail the predictions of the Reggeized pion exchange, we have calculated the  $A_L/A_0$  moments of the  $\pi^-p$ -vertex c.m. angular distribution for those events with  $|\cos\theta_{\Delta^{\text{c.m.}}}| > 0.965$ . These are the events used in calculating the moments shown in Figs. 19, 20, 27, and 28. The dashed curves in Fig. 19 are the predictions of Eqs. (21), (22), and (23a) using  $\alpha'=1$  GeV<sup>-2</sup> and  $S_0=1$  GeV<sup>2</sup>, and the on-shell  $d\sigma/d\Omega$ . The Regge calculations are seen to increase the value of the moments above the on-shell values for  $L>3$  throughout most of the mass range, in rough agreement with the experimental situation.

It should be noted that this calculation is approximate in that there is no cut applied to  $t$ , but rather a  $\cos\theta_{\Delta^{\text{c.m.}}}$  cut. This gives small contributions from  $t > 0.3$  GeV<sup>2</sup> at large  $m$  values. Furthermore, there is no cut on  $t_p$  made, which is necessary if one wants to compare the calculations with the conventional moments evaluated in the  $\pi^-p$  rest frames. This procedure is somewhat different from that used by Chien *et al.*,<sup>65</sup> who evaluated "quasi-moments" on the  $t_p$  cut sample of data which therefore did not span the full  $-1 < \cos\theta < +1$  range in the  $\pi^-p$  rest frame. The justification of our procedure is that there are few events with large  $t$  and the essential results are rather independent of this detail.

The predictions of the Regge model for the  $\langle \text{Re}Y_L^1 \rangle$  moments with  $L \leq 3$  are shown as the dashed curves in Figs. 27(a), 27(b), and 27(d). The corresponding  $\langle \text{Re}Y_L^1 \rangle$  moments for  $4 \leq L \leq 6$  are shown as the dashed

<sup>65</sup> C. Y. Chien, E. I. Malamud, D. J. Mellema, F. D. Rudnick, P. E. Schlein, W. E. Slater, D. H. Stork, H. K. Ticho, and T. G. Tripple, Phys. Letters 29B, 433 (1969).

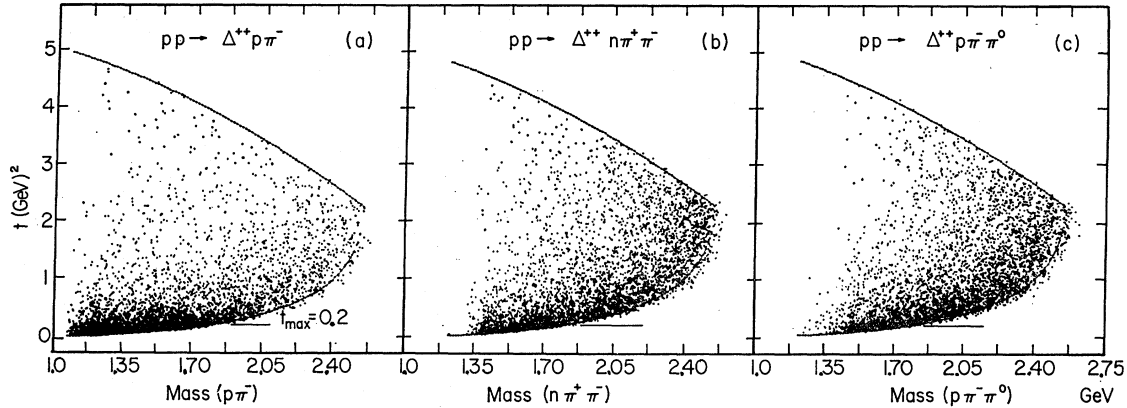


FIG. 31. Chew-Low plots of the type  $pp \rightarrow \Delta^{++}X$  for the indicated reactions. The  $\Delta^{++}$  selection is 1.14–1.30 GeV. If both  $p\pi^+$  mass combinations satisfy this selection, an event is plotted as two points.

curves in Figs. 28(a)–28(c). The agreement between the data points and the curves is reasonably good in all cases.

#### Proposed $\pi\Delta$ Final-State-Interaction Model

If, as seems to be the case, the pion trajectory is rather flat and  $\alpha' \approx 0$ , then the success of the Reggeized Deck-model calculation may be rather illusory. The fact that the inclusion of an explicit  $m_{\Delta\pi}$  dependence [in this case  $(m_{\Delta\pi}^2)^{2\alpha_\pi(t)}$ ] allows the shape of the  $m_{\Delta\pi}$  distribution to be fitted (and hence kinematically also

the  $\theta$  and  $\phi$  distributions) suggests that an alternative model is one in which a final-state  $\pi\Delta$  interaction leads to a change in *shape* of the  $\Delta\pi$  mass spectrum but not its magnitude. A multiplicative  $m_{\Delta\pi}$ -dependent factor  $f(m_{\Delta\pi})$  combined with DP-OPE would probably work,  $f(m_{\Delta\pi})$  would then contain information about the  $\Delta\pi$  interaction.

The desirability of this type of model over the Reggeized-pion-exchange type of model is that with the former one would be using an  $s$ -channel ( $\Delta\pi$ ) picture to describe the situation at low  $m_{\Delta\pi}$  values, which is essentially an  $s$ -channel dominated situation. The latter  $t$ -channel description depends for its validity (even if the pion-trajectory did have unit slope, which seems doubtful) on the detailed duality connection between  $s$ - and  $t$ -channel descriptions; it can at best be an approximate description of the low- $m_{\Delta\pi}$   $s$ -channel-dominated situation. Duality is an interesting and undoubtedly important concept, but why use an approximate  $t$ -channel picture to describe a situation whose  $s$ -channel aspects you are trying to learn, as in  $\pi p \rightarrow (\rho\pi)p$  and  $Kp \rightarrow (K^*\pi)p$ ? If a final-state-interaction model can be set up and made to work for a case where we “know” the  $s$ -channel interaction [i.e.,  $pp \rightarrow (\Delta^{++}\pi^-)p$ ], the model could then be applied to those cases where we would like to learn about the  $s$ -channel interactions ( $\rho\pi$  and  $K^*\pi$ ).

#### F. Comparison between On- and Off-Mass-Shell Inelasticities in $\pi^-p$ Scattering

For completeness, we include here a brief summary of a comparison we have made<sup>12</sup> among the three reactions

$$pp \rightarrow \Delta^{++}(p\pi^-), \quad (27a)$$

$$pp \rightarrow \Delta^{++}(n\pi^+\pi^-), \quad (27b)$$

$$pp \rightarrow \Delta^{++}(p\pi^-\pi^0) \quad (27c)$$

for low momentum transfer to the  $\Delta^{++}$  ( $t < 0.2$  GeV<sup>2</sup>).

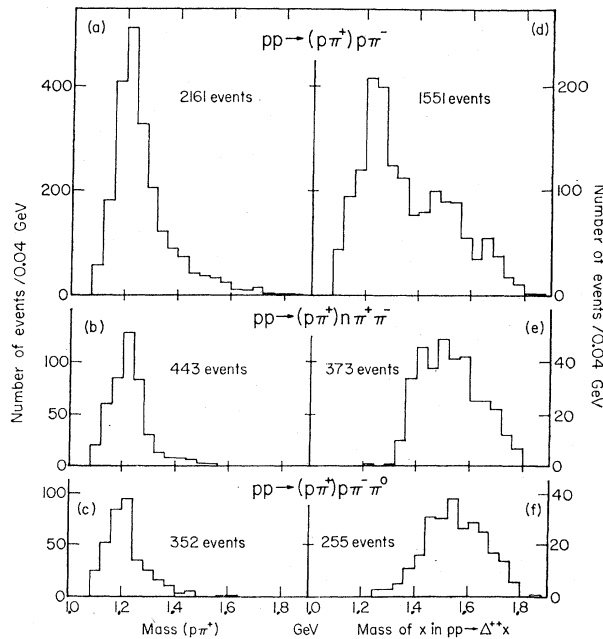


FIG. 32. (a)–(c)  $p\pi^+$  mass projections for momentum transfer to the  $p\pi^+$  system  $t < 0.2$  GeV<sup>2</sup>. Only one  $p\pi^+$  combination is plotted for each event (the combination with lower  $t$ ). (d)–(f) Mass projection for the  $X$  system in  $pp \rightarrow \Delta^{++}X$  for the indicated reactions using the 1.14- to 1.30-GeV  $\Delta^{++}$  selection and for  $t < 0.2$  GeV<sup>2</sup>.



The Chew-Low plots for these reactions, shown in Fig. 31, demonstrate the peripheral character of reactions (27b) and (27c). Figure 32 compares the low-momentum transfer  $p\pi^+$  and non- $\Delta^{++}$  mass spectra for each of these reactions. In Fig. 33 is shown the ratio of the cross sections

$$\sigma(\Delta^{++}p\pi^-\pi^0)/\sigma(\Delta^{++}p\pi^-)$$

and

$$\sigma(\Delta^{++}n\pi^+\pi^-)/\sigma(\Delta^{++}p\pi^-)$$

as a function of mass of the non- $\Delta^{++}$  system. The shaded bands in each figure represent the known on-shell cross-section ratios  $\sigma(\pi^-p \rightarrow p\pi^-\pi^0)/\sigma(\pi^-p \rightarrow \pi^-p)$  and  $\sigma(\pi^-p \rightarrow n\pi^-\pi^+)/\sigma(\pi^-p \rightarrow \pi^-p)$ .

The observed agreement between the shaded bands and the data<sup>66</sup> in Fig. 33 suggest that (a) reactions (27b) and (27c) are pion-exchange dominated (in the selected low- $t$  region) and proceed via the same type of process illustrated in Fig. 17 but with the off-shell inelastic  $\pi^-p \rightarrow n\pi^-\pi^-$  and  $\pi^-p \rightarrow p\pi^-\pi^0$  at the upper vertex; (b) the off-shell corrections to the pion-exchange pole equation for reactions (27b) and (27c) are similar to the DP factors which describe reaction (27a) rather well. Only if the  $t$  dependences of the various inelastic processes were similar could the ratios of the cross sections in the physical region of the Chew-Low plane agree with the on-shell ratios.<sup>67,68</sup> It is for essentially the same reason that the  $\pi\pi$  phase shifts and  $t$  dependences obtained in the reaction<sup>69</sup>

$$\pi^-p \rightarrow \pi^-\pi^+n \quad (28)$$

can be used to predict rather well the Chew-Low distribution for the reaction<sup>70</sup>

$$\pi^-p \rightarrow \pi^0\pi^0n. \quad (29)$$

## IX. CONCLUSIONS

The peripheral three-body process  $p\bar{p} \rightarrow \Delta^{++}(1238)p\pi^-$  accounts for 80% of the events, with evidence for simultaneous  $\Delta^0(1238)$ ,  $N^{*0}(1512)$ , and  $N^{*0}(1688)$  resonance production in the  $\pi^-p$  mass

<sup>66</sup> Note, as in Ref. 12, that the small discrepancy between the data and the shaded band in Fig. 33 for  $p\pi^-\pi^0/p\pi^-$  can be understood as being due to a non- $\Delta^{++}$  background seen in Fig. 32(c). Such a background does not appear to exist for the  $\Delta^{++}n\pi^+\pi^-$  reaction.

<sup>67</sup> We have also found agreement between the relative yields of the low-momentum transfer components of the reaction  $p\bar{p} \rightarrow \Delta^{++}$  (neutrals) and  $p\bar{p} \rightarrow \Delta^{++}(\pi^-p)$  (at 6.6 GeV/c) and the relative cross sections for  $\pi^-p \rightarrow$  neutrals and  $\pi^-p \rightarrow \pi^-p$ . See, e.g., E. Colton *et al.*, Phys. Rev. D **2**, 2108 (1970).

<sup>68</sup> Similar results have also been obtained in comparisons of  $p\bar{p} \rightarrow \Delta^{++}+M$  reactions at 28.5 GeV/c. See, e.g., W. E. Ellis *et al.*, Phys. Letters **32B**, 140 (1970).

<sup>69</sup> E. Malamud and P. E. Schlein, Phys. Rev. Letters **19**, 1056 (1967); in *Proceedings of the Conference on  $\pi\pi$  and  $K\pi$  Interactions* (Argonne National Laboratory, Argonne, Ill., 1969), p. 93.

<sup>70</sup> G. A. Smith and R. J. Manning, Phys. Rev. Letters **23**, 335 (1969); K. J. Brown, D. Cline, and V. Scherer, *ibid.* **21**, 1275 (1968); P. Sonderegger and P. Bonamy, in *Proceedings of the Lund International Conference on Elementary Particles, 1969*, edited by G. von Dardel (Berlingska, Boktryckeriet, Lund, Sweden, 1969).

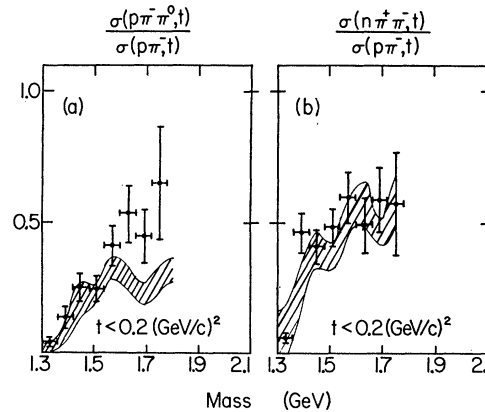


FIG. 33. (a) Ratio of the cross section for  $(p\bar{p} \rightarrow \Delta^{++}p\pi^-\pi^0)/(\bar{p}p \rightarrow \Delta^{++}p\pi^-)$  as a function of the mass of the non- $\Delta^{++}$  final-state system, where the momentum transfer to the  $\Delta^{++}$  is  $t < 0.2$  GeV<sup>2</sup>. (b) The same for  $(p\bar{p} \rightarrow \Delta^{++}n\pi^+\pi^-)/(\bar{p}p \rightarrow \Delta^{++}p\pi^-)$ . The shaded bands represent a summary of the known experimental ratios  $(\pi^-p \rightarrow p\pi^-\pi^0)/(\pi^-p \rightarrow \pi^-p)$  and  $(\pi^-p \rightarrow n\pi^+\pi^-)/(\pi^-p \rightarrow \pi^-p)$ , respectively.

spectrum. The peripheral  $\Delta^{++}\pi^-$  mass spectrum displays a Deck-type enhancement in the region of 1450 MeV, thought by some to be production of the  $P_{11}$  ‘‘Roper Resonance’’; however, the angular correlations observed in the breakup of our enhancement appear not to be consistent with the decay of a pure  $J^P = \frac{1}{2}^+$  state. Approximately 10% of the events in our total sample involve production of  $N^{*+}(1700)$  resonances in the reaction  $p\bar{p} \rightarrow pN^{*+}$ . We also find evidence for small percentages of  $\rho^0$  and  $f^0$  meson production in the reactions  $p\bar{p} \rightarrow p\bar{p}\rho^0$  and  $p\bar{p} \rightarrow p\bar{p}f^0$ .

Three types of analyses are presented which strongly imply that the OPE process illustrated in Fig. 17 is dominantly responsible for  $p\bar{p} \rightarrow \Delta^{++}p\pi^-$ , at least in the low-momentum-transfer region. These analyses have to do with (a) angular correlations in the  $\pi^\pm p$  rest frame being similar to those found in on-shell  $\pi^\pm p$  scattering; (b) extrapolation of the observed Chew-Low distribution to the pion-exchange pole leads to correct on-shell  $\pi p$  elastic-scattering cross sections (the  $t$  dependence used in the extrapolation for  $\pi^-p$  mass  $m > 1.6$  GeV is the same as that observed in other pion-exchange reactions involving  $\Delta^{++}$  production); (c) relative cross sections for low-momentum-transfer production of  $(p\pi^-\pi^0)\Delta^{++}$ ,  $(n\pi^-\pi^+)\Delta^{++}$ , and  $(\pi^-p)\Delta^{++}$  are found to agree within errors with the on-shell inelastic cross-section ratios for  $p\pi^-\pi^0$ ,  $n\pi^-\pi^+$ , and  $\pi^-p$  in  $\pi^-p$  scattering.

The  $\Delta^{++}\pi^-$  mass spectrum with its rather spectacular Deck effect (peak at low  $\Delta^{++}\pi^-$  mass when large  $\pi^-p$  mass is selected) is thus dominantly accountable for *in magnitude* by the OPE process. In particular, the observed Chew-Low distribution in  $\pi^-p$  mass and momentum transfer to the  $\Delta^{++}$ ,  $d^2\sigma/dt dm$ , is described by the pole equation modified by the Dürre-Pilkuhn factor at the  $\Delta^{++}$  vertex.

A detailed study is made of the shape of the  $\Delta^{++}\pi^-$  mass spectrum. Although the area is accounted for with the pion-exchange picture, the shape can only be fitted in detail if a modest *ad hoc* dependence on  $m_{\Delta\pi}$  is introduced or, equivalently, if the  $\theta, \phi$  distribution at the  $\pi^-p$  vertex is modified from the on-shell distribution in such a way as to agree with the observed  $\theta, \phi$  distribution. This latter possibility might be accomplished with an absorption model appropriate for the three-body final state; however, we know of no such model and therefore have not pursued this possibility.

Two ways in which an *ad hoc* dependence on  $m_{\Delta\pi}$  can be introduced are the following. (a) Reggeize the exchange pion as in the model of Berger. Although the model fits all the experimental distributions rather well, including the  $m_{\Delta\pi}$  distribution and the Treiman-Yang angular dependence at the  $\pi^-p$  vertex, a difficulty is that the pion trajectory with unit slope required by the model seems to be at variance with the relatively flat trajectory deduced from quasi-two-body data by Wolf<sup>46</sup> and by Boyarski *et al.*<sup>61</sup>. (b) Introduce a final-state  $\Delta\pi$  interaction which modifies the shape of the  $m_{\Delta\pi}$  distribution but does not alter the cross section significantly. It would be interesting to see such a model formulated.

Clearly, further experimental work is needed on the determination of the pion trajectory. If, as present evidence on this subject seems to indicate, the trajectory is rather flat and close to zero, then our so-called "un-Reggeized" Deck calculation based on  $(d^2\sigma/dtdm)_{\text{D.F.O.P.E}}$  combined with the on-shell  $\theta, \phi$  distribution at the  $\pi^-p$  vertex is actually the valid "Reggeized" calculation.

The Deck situation in  $p\pi^-\Delta^{++}$  seems to be different from that of the  $Q$  enhancement in  $K^+p \rightarrow K^{*0}\pi^+p$ . In the latter case the magnitude of the  $Q$  enhancement is significantly larger than can be understood as due to pion exchange.<sup>71</sup> This may perhaps be due to the additional contribution of  $K^*$  exchange or perhaps equivalently to the fact that the final-state  $K^*\pi$  inter-

action is significantly larger than the  $\Delta\pi$  interaction, a fact which results in an increase in the cross section.

In conclusion then, the  $\sim 1450$ -MeV Deck enhancement in  $p\pi^- \rightarrow p\pi^-\Delta^{++}$  appears not to have the angular correlation properties of a pure  $J^P = \frac{1}{2}^+$  state. Its magnitude is accountable for in terms of the aforementioned pion-exchange process, indicating that only one process is responsible for the production of  $p\pi^-\Delta^{++}$  and *not* pion exchange plus diffraction production of the Deck enhancement. This point was made earlier by us in Ref. 11. A (relatively weak) *ad hoc*  $m_{\Delta\pi}$  dependence must be added to fit in detail the shape of the  $m_{\Delta\pi}$  dependence or, equivalently, the angular distribution at the  $\pi^-p$  vertex. If we accept the present evidence for a rather flat pion trajectory, the success of the Berger Reggeized Deck model indicates that it is possible to introduce an explicit *ad hoc*  $m_{\Delta\pi}$  dependence and obtain the required (implicit) dependence on  $\theta, \phi$  to fit the data. This would then have important implications for the potential success of a  $\Delta\pi$  final-state-interaction model.

Further analyses of the  $p\pi^- \rightarrow p\pi^-\Delta^{++}$  reaction with higher statistics and at other beam momenta would be useful.

#### ACKNOWLEDGMENTS

We wish to thank H. K. Ticho and S. Wojcicki for their participation in the early stages of this experiment and W. Chinowsky, who designed and built the P65 beam. We also thank Luis Alvarez for his continuing support and cooperation. In addition, we thank Gunther Wolf, Bob Panvini, and Tom Morris for helpful discussions and for communicating results to us prior to publication. One of us (E.C.) is grateful for the help given by Chih-Yung Chien in the Reggeized Deck model calculation. This experiment would not have been possible without the efforts of Robert Watt and the entire crew of the 72-in. bubble chamber. Finally the work of the scanners, programmers, draftsmen, and photographers of both the Lawrence Radiation Laboratory and the University of California, Los Angeles is gratefully acknowledged.

<sup>71</sup> T. G. Trippe, UCLA 7.3-GeV/c  $K^+p$  group (private communication).